THE UNIVERSITY OF MICHIGAN
COLLEGE OF LITERATURE, SCIENCE, AND THE ARTS
Department of Physics

Technical Report No. 10

PION-PROTON ELASTIC SCATTERING FROM 3 GEV/C TO 5 GEV/C

M. L. Perl
L. W. Jones
C. C. Ting

ORA Project 03106

under contract with:

DEPARTMENT OF THE NAVY
OFFICE OF NAVAL RESEARCH
CONTRACT NO. Nonr-1224(23)
WASHINGTON, D.C.

administered through:

OFFICE OF RESEARCH ADMINISTRATION ANN ARBOR

June 1963

This report consists of a paper prepared
for submission to the PHYSICAL REVIEW.

TABLE OF CONTENTS

ABSTRACT

Results of a spark chamber experiment on elastic scattering of pions on protons are presented and analyzed. The processes studied were π^+ p at 2.92 GeV/c, and π^- p at 3.15, 4.13, and 4.95 GeV/c. The data are fit to an exponential function of the four-momentum transfer, t, in several different ways in attempts to explore systematic energy and angular dependences. No shrinkage of the diffraction peak is seen in comparing the coefficients of a linear exponential fit for $|t| < 0.4$ $(\text{GeV/c})^2$; at larger $|t|$, however, the cross section falls off with increasing energy. The large angle differential cross section is examined for structure, and is compared with all other large angle scattering data. The results are compared with proton-proton scattering data over the same energy range and substantial differences between the two processes are evident.

I. INTRODUCTION

This paper reports the results of measurements of the elastic differential cross section of π^- mesons on protons at 3.15, 4.13, and 4.95 GeV/c, and of π^+ mesons on protons at 2.92 GeV/c. These measurements are compared with other published pion-proton elastic scattering data at similar and higher energies and with proton-proton elastic scattering results. The relevant theories are reviewed and examined in the light of these data.

The results of the measurements of the diffraction-peak part of the differential cross section have already been reported.[1] They were interpreted with respect to the Regge theory of elastic scattering and the conclusion was that although the diffraction peaks had, at least approximately, the predicted exponential behavior, there was little or no evidence for the predicted shrinking of the π^- p diffraction peaks with increasing energy. Higher-energy measurements of the π^- p elastic diffraction peak[2] subsequently confirmed the non-existence of the shrinkage. Section V of this paper is devoted to a further discussion of the diffraction peak results, mostly with respect to the precise shape of the diffraction peak.

This experiment used thin-plate spark chambers and a liquid hydrogen target and was carried out at the Bevatron of the Lawrence Radiation Laboratory. The apparatus and method of analysis are briefly described in Section III. In Section IV completely analyzed results of the experiment are tabulated and plotted. Section VI is devoted to a discussion of the large-angle scattering, for which only very preliminary results have been pub-

lished.[3] In Section VII pion-proton and proton-proton scattering are compared and discussed. Throughout this paper, all kinematical quantities and differential cross sections are in center-of-mass systems; energies are given in GeV, momenta in GeV/c, distances in cm, and wave numbers in cm^{-1} unless otherwise indicated. An exception is the laboratory momentum of the incident pion which is used to specify each of the four sets of data.

Before discussing specific theories, it is useful to recall the features of high-energy pion-nucleon elastic scattering. The first distinctive feature of pion-nucleon elastic scattering when the laboratory momentum of the incident particle is above 2 GeV/c is a narrow forward peak which contains almost all of the total elastic cross section. This same feature occurs in all other instances of high-energy elementary-particle elastic scattering which have been measured thus far: for example, p p,[4,5] $\bar{p}$ p,[6] and K^+ p.[7] The second distinctive feature of pion-nucleon elastic scattering is characteristic of all other measured system as well: the total elastic cross section is a rather slowly varying function of energy compared with any particular inelastic channel. As examples of these features at 5 GeV/c, the π^- p differential cross section, which has a value of about 30 mb/sr in the center-of-mass system at 0°, drops to one-tenth of its value at 21° and to one-hundredth of its value at 32°. Furthermore the forward peak contains at least 95% of the total elastic cross section up to 32°. The total elastic cross section at 5 GeV/c is 6.5 mb, whereas at 10 GeV/c it is 4.6 mb.[8] This forward peak may be interpreted as diffraction scattering, noting that in this range of momenta the wavelength of the pion is of the

order of or less than the nucleon radius. The diffraction peak follows classically from the imaginary scattering amplitudes corresponding to the various inelastic channels.

While the diffraction analogy justifies the existence of a forward peak, it does not explain the very small elastic differential cross section at large angles; that is, it does not explain why almost all elastic scattering is diffractive. An admittedly weak explanation is that as the energy increases substantially the total cross section of any particular channel usually decreases rapidly. There is nothing special about the elastic channel, and therefore its total cross section should decrease rapidly, except that the diffraction requirements "force" the elastic scattering to stay large in the forward direction. Part of this argument is made explicit in the "statistical model theory" of large-angle scattering given in Section II.

Most of the theoretical work has been concerned with the diffraction region, where data are more abundant and theoretical treatment is more straightforward. Convenient kinematical parameters for describing the process are s, t, and u, defined as follows in terms of incident pion and proton four-momenta, q_1 and p_1 respectively, and of the corresponding outgoing four-momenta, q_2 and p_2:

$$\begin{aligned} s &= (p_1 + q_1)^2 \\ t &= (p_1 - p_2)^2 \\ u &= (p_1 - q_2)^2 \,. \end{aligned} \tag{1}$$

The variable s is the square of the total c.m. energy; and t is the square of the four-momentum transfer, given also by

$$t = -2|\underset{\sim}{q}|^2 (1 - \cos \theta) , \qquad (2)$$

where $\underset{\sim}{q}$ is the three-momentum and θ is the scattering angle of the pion. For purposes of discussion we designate the diffraction region as the range of θ for which $|t| < 0.8$ $(\text{GeV}/c)^2$. While no break in the cross section exists at this value, it is found that almost all of the forward elastic peak is included in this t-region and that the diffraction region theoreies are expected to hold best for this region. When comparing the pion-proton with the proton-proton system we shall use this same separation point.

A large-angle scattering region of particular interest which occurs in pion-proton and other elastic scattering of unlike particles (but not in proton-proton scattering) is the region near $\theta = 180°$. As described in Section II, this region is supposed to be dominated by processes completely different from those which produce the diffraction peak. There has been particular interest in the possibility of a backward peak near 180°.

II. THEORIES OF PION-NUCLEON ELASTIC SCATTERING

A. General Consideration

1. Isotopic spin dependence.—Pomeranchuk[9] and others have shown that as the energy increases, the total π^+ p and π^- p cross sections should become equal. There is no proof that the total elastic cross sections or the

differential cross sections should become equal, but all the theories of scattering outlined below indicate strongly that the diffraction scattering should become independent of isotopic spin. This is probably not true for large-angle scattering, particularly for the 180° region where the major differences discussed below might be expected to occur.

2. Forward elastic scattering.—The scattering amplitude is defined by

$$\frac{d\sigma}{d\Omega}(\theta) = |f(\theta)|^2 , \tag{3}$$

and the optical theorem states, neglecting coulomb scattering,

$$\text{Im } f(\theta) = \frac{k}{4\pi} \sigma_{tot} , \tag{4}$$

where $k = |\underset{\sim}{q}|/\hbar$. Then

$$\frac{d\sigma}{d\Omega}(\theta) = |\text{Re } f(\theta)|^2 + \frac{k^2}{16\pi^2} \sigma_{tot}^2 . \tag{5}$$

It is usually assumed from rough measurements and from calculations using forward dispersion relations that the Re $f(\theta)$ is small compared with the Im $f(\theta)$. This assumption will be tested again with the present data, but most of the diffraction theories are based on a purely imaginary value of $f(\theta)$.

B. Theories of Diffraction Scattering

1. Optical model.—The partial wave expansion for the scattering amplitude is

$$f(\theta) = \frac{1}{2ik} \sum_{\ell=0}^{\infty} (2\ell+1)(1-\eta_\ell) P_\ell(\cos\theta) . \tag{6}$$

The simplest derivation of the diffraction peak is then obtained (as shown in the Appendix) by setting

$$L = kR$$

$$\eta_\ell = a \qquad 0 \leq \ell \leq L$$

and

$$\eta_\ell = 0 \qquad \ell > L \,, \tag{7}$$

where a, which is real and less than 1, is the amplitude of the transmitted wave from a unit incident wave. The quantity (1-a) is then the "opacity" and R is the radius of the proton in this simple model.

The following results are obtained for the diffraction region:

$$f(\theta) = \frac{(1-a)kR^2}{2}$$

$$\frac{d\sigma}{d\Omega}(\theta) = (1-a)^2 R^4 k^2 \left[\frac{J_1(kR\theta)}{kR\theta}\right]^2 \tag{8}$$

$$\sigma_{tot} = 2\pi(1-a)R^2 \,.$$

Although a more sophisticated optical model can be made,[10] we will use only the simple Eqs. (8) since our primary purpose is to compare the fitted parameters R and (1-a) of the p p diffraction peak with those of the π p diffraction peak.

2. Theories based on the Mandelstam Representation.—All relativistic and field theoretic descriptions of elastic scattering have come at least partially from the Mandelstam representation. The basic idea, that the scattering amplitude is to be derived by studying the singularities in the cross channels which are the pion-pion system, has been discussed in detail

by Chew.[11] Diffractive scattering in terms of the singularities of the pion-pion system alone has been studied by a number of authors.[12,13] The general reasoning is based on the fact that the diffraction peak occurs at small negative values of t and the pion-pion singularities occur at small positive values of t, whereas the crossed-channel pion-nucleon singularities occur at very large negative values of t. The supposition is then made that the diffraction peak can be understood in terms of closely-lying pion-pion singularities. We may replace $f(\theta)$ by $f(s,t)$ and factor out the $t = 0$ behavior of $f(s,t)$ so that

$$\frac{d\sigma}{d\Omega} = [f(s,t)]^2 = [f(s,0)]^2 \left[\frac{f(s,t)}{f(s,0)}\right]^2 . \tag{9}$$

Setting $f(s,t)/f(s,0) = F(s,t)$ yields

$$\frac{d\sigma}{d\Omega} = f(s,0)^2 F(s,t) . \tag{10}$$

Finally,

$$\frac{d\sigma}{d\Omega} = - \frac{|\underset{\sim}{q}|^2}{\pi} \frac{d\sigma}{dt} \tag{11}$$

so that

$$- \frac{d\sigma}{dt} = \left[\frac{\pi}{|\underset{\sim}{q}|^2} |f(s,0)|^2\right] F(s,t) = - \left(\frac{d\sigma}{dt}\right)_0 F(s,t) . \tag{12}$$

The high-energy approximation Re $f(s,0) = 0$ and Eq. (5) yields

$$- \frac{d\sigma}{dt} = \frac{\sigma_{tot}^2}{16\pi\hbar^2} F(s,t) . \tag{13}$$

Now the observation of high-energy diffraction scattering has shown that

F(s,t), i.e., the shape of the diffraction peak, is not very energy-dependent. Therefore the aim of relativistic diffraction theories has been to produce an F(s,t) in which the s-dependence is small and the t-dependence not only fits the data but has some justification from the Mandelstam representation. This has been done by Amati et al.,[12] and by Lovelace.[13] With our data the s-dependence can be only roughly examined, and we will confine ourselves to the simplest Regge theory in examining it. Even if the Regge theory were not right it would still provide a convenient way to parameterize the s- and t-dependence of the elastic scattering.

3. The Regge theory.—According to the ideas of Chew and Frautschi,[14] Frautschi et al.,[15] and Drell,[16] pion-nucleon diffraction scattering may be explained by the P (Pomeranchuk or Vacuum), P' (Pomeranchuk prime), and ρ trajectories. The scattering amplitude for large s and small |t| is written

$$f(s,t) = \frac{1}{8\pi\sqrt{s}} \sum_i \beta_i(t)\,(s/s_0)^{\alpha_i(t)}, \qquad (14)$$

where the i sums over all the trajectories. While this f(s,t) has a limited type of s-dependence, there are too many unknown functions to allow testing of the theory by present diffraction data. Thus Eq. (14) could fit almost any data.

The applicability of the simple Regge theory to the diffraction scattering problem has recently been brought into serious doubt, not only by high-energy elastic scattering data[2] but also by unpublished calculations reported to demonstrate the existence of cuts in the complex α (angular momentum) plane.

The number of unknown functions can be reduced by assuming that at large s the P trajectory is the most important one since for small $|t|$, $\alpha_P(t)$ is larger than other $\alpha_i(t)$. Keeping only the term containing the next largest α, say α_1, we may write

$$f(s,t) = \frac{1}{8\pi\sqrt{s}}\left[\beta_P(t)\ (s/s_0)^{\alpha_P(t)} + \beta_1(t)\ (s/s_0)^{\alpha_1(t)}\right],$$
$$f(s,0) = \frac{1}{8\pi\sqrt{s}}\left[\beta_P(0)\ (s/s_0)^{\alpha_P(0)} + \beta_1(0)\ (s/s_0)^{\alpha_1(0)}\right]. \tag{15}$$

Assuming $\alpha_P(0) = 1$, the first two terms in $F(s,t)$ are

$$F(s,t) \cong \left|\frac{\beta_P(t)}{\beta_P(0)}\right|^2 (s/s_0)^{2\alpha_P(t)-2} + \left\{\frac{2\mathrm{Re}[\beta_P(t)\beta_1^*(t)]}{|\beta_P(0)|^2}\right\}(s/s_0)^{\alpha_P(t)+\alpha_P(t)-2} . \tag{16}$$

Lacking knowledge of the $\beta(t)$, these two terms can be separated only by their s-dependences. However, the observed s-dependence of F is small. This $F(s,t)$ may be rewritten making use of the following assumptions. Considering $\alpha_P(t) = \alpha_1(t)+\Delta$, Eq. (16) can be factored to the following functional form:

$$F(s,t) \cong \left|\frac{\beta_P(t)}{\beta_P(0)}\right|^2 (s/s_0)^{2\alpha_P(t)-2}[1+g(t)\,s^{-\Delta}] . \tag{17}$$

In the case of the P' trajectory, Δ is presumed to be about 0.5. Thus, although it is predicted that the diffraction scattering peak due to the Pomeranchuk trajectory will shrink with increasing energy, the situation may be altered by the presence of terms from other trajectories. Only the leading term will be kept in the following discussion, although the parameterization of Eqs. (16) and (17) should be borne in mind. This same point has

been made by Hadjioannou et al.,[17] in discussing the t-dependence of p p diffraction scattering.

Continuing with the Pomeranchuk trajectory alone, we may drop the subscript P and write

$$\frac{d\sigma}{dt} \cong \left(\frac{d\sigma}{dt}\right)_{t=0} \left| \frac{\beta(t)}{\beta(0)} \right|^2 (s/s_0)^{2\alpha(t)-2} . \tag{18}$$

For small $|t|$, the experimental data are well fit by

$$\frac{d\sigma}{dt} = \left(\frac{d\sigma}{dt}\right)_{t=0} \exp[A(s)t] . \tag{19}$$

Thus, if

$$\alpha(t) = 1+\alpha'(0)t, \quad \text{and} \quad \beta(t) = \beta(0) \exp[\eta t]$$

we may write

$$\frac{d\sigma}{dt} = \left(\frac{d\sigma}{dt}\right)_{t=0} \exp[\gamma+2\alpha'(0) \ln s\, t] \tag{20}$$

where

$$\gamma = \eta - 2\alpha'(0) \ln s_0 .$$

C. Theories of Large-Angle Scattering

1. The statistical model theory.—Fast et al.,[18] have calculated the cross section for elastic scattering with the scattering considered as just one of the many final-state channels occurring in the statistical model of high-energy elementary-particle collisions. The statistical model is concerned with central and not with peripheral collisions. Therefore it may

yield that part of the elastic cross section which is not given by the diffraction theories, all of which are concerned with peripheral collisions. In effect, the statistical model assumes some probability for a "time-like" intermediate state: an excited or "compound" nucleon. This is in contrast to the "space-like" intermediate state, or propagator, of peripheral models. Time-like intermediate states appear to be a valid physical concept at energies below 2 GeV (the resonance region). The question of the validity of the statistical model may be interpreted as asking whether the probability for the formation of time-like intermediate states falls off only slowly with increasing energy and whether it is through these states that some rare final states, such as large-angle elastic scattering, are reached at high energy. Fast et al.,[18] find that the total non-diffractional cross section decreases exponentially with increasing center-of-mass energy, according to the exponent ($-3.17\ E_{c.m.}$). They assume the angular distribution to be isotropic in the center-of-mass system.

2. Backward peak from partial wave expansion.--Blokhintsev[19] has shown how the same assumptions which lead to the diffraction peak also lead to a peak at 180°. We have given an alternative derivation in the Appendix, where we show that if

$$\theta' = 180° - \theta ,$$

then

$$\frac{d\sigma}{d\Omega}(\theta') = (1-a)^2 R^2 [B(kR\theta')]^2 , \qquad (21)$$

where $B(kR\theta)^2$ is a function plotted in Fig. 1 for comparison with the diffraction-peak function $[J_1(kR\theta)/kR\theta]^2$. The ratio of the backward-peak height at 180° to the forward-peak height at 0° is $1/k^2R^2$, and since kR is the maximum angular momentum L which enters the reaction, the backward peak is $1/L^2$ times the height of the forward peak. Since L = kR at, say, 4 GeV/c $\cong$ 10, the backward peak predicted in this way is quite small in comparison with the forward peak. The total backward elastic scattering cross section in this peak is

$$\sigma_{\text{elastic backward peak}} = .78(1-a)^2\pi\lambda^2 . \qquad (22)$$

Thus this theory predicts a small backward elastic peak whose total cross section goes inversely as k^2 or approximately inversely as s. We shall examine the data with reference to the existence of such a peak.

3. Backward peak from a neutron or nucleon isobar pole.—As stated earlier, in principle the elastic scattering near 180° should be calculable from singularities in the cross pion-nucleon channel. The relevant relativistic invariant is now u, where

$$u = \frac{(M^2-m^2)}{s} - 2\,|\underset{\sim}{q}|^2\,(1+\cos\theta) . \qquad (23)$$

Here M is the proton mass and m the pion mass. It will be noticed that unlike t, which is 0 at $\theta = 0$ and is always negative in the physical region, $u = (M^2-m^2)^2/s$ at $\theta = 180°$ and is negative only for

$$\cos\theta > \frac{(M^2-m^2)}{2|\underset{\sim}{q}|^2\,s} - 1 . \qquad (24)$$

Singh and Udgaonkar[20] have discussed briefly the backward peak to be expected on the basis of the strip approximation to the Mandelstam representation. They estimate that the width of the peak in terms of u should be about four times the width of the forward peak in terms of t. At 4 GeV/c the half-width would be 0.4 $(\text{GeV/c})^2$ in terms of u or 0.12 in terms of cos Θ.

Several authors have conjectured that π^+ p elastic scattering near 180° might be attributed mostly to a neutron exchange (Fig. 2a). If this very simplified way of using the singularities of the cross pion-proton channel is valid, π^- p elastic scattering near 180° might be attributed mainly to the exchange of the 3/2, 3/2 nucleon isobar (Fig. 2b). In these surmises the hope is that higher-order diagrams such as the 3/2, 3/2 isobar for π^+ p and Fig. 2c for both π^+ p and π^- p will not change the result much. But Cook et al.,[21] have shown that in π^+ p, 180° scattering the calculation based solely on neutron exchange gives the absurdly large answer of 90 mb/sr. Clearly, then, the other diagrams must be considered. No one has found specific means of doing so, but an unpublished calculation of Pomeranchuk[22] gives the π^+ p, 180° differential cross section as about 1 mb/sr. We will compare this prediction with our data, although the means of calculation is not known to us.

4. Regge theory for large angles.—The differential cross section at large $|t|$ values can be fitted by Regge trajectories in the t-channel because as shown in Eq. (17) there is considerable freedom in the large $|t|$ predictions. The question arises of how the amplitudes from the t- and u-channels can be combined if the values of u are of the same order of magnitude as the

values of t.

One solution is to follow Drell's suggestion[16] and assume that the amplitudes from the u-trajectories are very small in comparison with those from the t-trajectory. Here we are saying in another way what was said in the last section: from the standpoint of both Mandelstam theory and Regge theory, the u-channel somehow contributes very little to the large-angle elastic scattering, except perhaps near 180°. Therefore we will continue the s,t parameterization discussed in Section II.B.4 into the large-angle region, out approximately as far as $|t| \cong 2$ GeV/c. In the proton-proton case the shrinkage of the forward peak is most apparent at large t-values, which are outside the diffraction region. We shall see if this is also true for the pion-proton case.

One may explore the contribution of u-channel trajectories near θ = 180°. In particular, translating the discussion of Section II.C.3 into the Regge language, in π^+ p, 180° scattering we would hope to investigate the Regge neutron trajectory.

The kinematic relation (24) causes a difficulty in the Regge treatment of the u-channel. The basic idea of the Regge theory is that the cosine of the scattering angle in the cross channel should be much greater than 1. For the t-channel,

$$\cos \theta_t \to 1 + \frac{s-[(t/4-m^2)^{1/2}-(t/4-M^2)^{1/2}]^2}{2(t/4-m^2)^{1/2}(t/4-M^2)^{1/2}} \quad . \qquad (25)$$

In the forward peak, $s \gg t$ and thus $\cos \theta_t \gg 1$ for $s \gg Mm$; but for the u-channel,

$$\cos \theta_u \to - \left[1 + \frac{2[su-(m^2-M^2)^2]}{(u-m^2-M^2)^2-4m^2M^2} \right] . \qquad (26)$$

At $u = (M^2-m^2)^2/s$, i.e., at $\theta = 180°$, $\cos \theta_u = -1$ for all s, and at $u = 0$, $\cos \theta_u = +1$ for all s. To obtain a "large" value of $\cos \theta_u$, say 3 or 10, requires a fairly large value of $|u|$ as given in Table I. Now the Regge theory gives a simple forward-peak prediction, once the Pomeranchuk trajectory is taken as dominant, because for small $|t|$, $\alpha_P(t)$ can be taken as linear and the theory holds best at $t = 0$, which corresponds to $\theta = 0$. But in the backward hemisphere there is the ambiguous region extending from $\theta = 180°$ to the angles listed in Table I at which $\cos \theta_u$ becomes large; and this includes the region of small u, where the Regge theory would otherwise be most applicable. Therefore Regge predictions of a backward peak, interpretable as a nucleon or nucleon isobar trajectory, are vague. In particular, predictions of the s-behavior, analogous to the predicted shrinkage with increasing s of the forward peak, seem difficult. It is only at energies much higher than those in this experiment, i.e., cases in which the ambiguous region has shrunk considerably, that the Regge predictions become clearer. Therefore in spite of the great interest in finding an effect of the nucleon or nucleon isobar Regge trajectory at 180° pion-proton scattering, our data force us to ignore this question unless the Regge predictions are clarified.

III. APPARATUS AND METHOD OF ANALYSIS

The pion beams were obtained from the Bevatron of the Lawrence Radiation Laboratory. The π^- beam was produced at 0° inside the Bevatron magnet and the π^+ beam was produced at 26° in a straight section. This large production angle limited the maximum π^+ momentum to 3 GeV/c and led to difficulties in normalization of the π^+ data due to proton contamination of the beam. The momentum spread of the beam was ±3% at half maximum for the π^- p and somewhat larger for the π^+ p.

Figure 3 shows a schematic horizontal view of the equipment.[23] The two small spark chambers 1 and 2 measure the angle of the incident pion. The double spark chambers 3, 3' and 4, 4' measure the angles of tracks going out the sides. The spark chambers 5 and 6 are spaced 2 ft apart in order to give a good angular measurement of forward-going particles. The scintillation counters in Fig. 3 were operated in coincidence circuits so that a signal had to be received in coincidence by at least one left-hand and one right-hand counter in order to pulse the spark chambers and record a photograph.

Using a combination of mirrors, the vertical and horizontal projections of the tracks in all spark chambers were imaged onto a single 35-mm film frame. A typical elastic scattering event is reproduced in Fig. 4. Since the counters were designed to accept particles from every point in the target making an angle of ±15° with the horizontal plane, the photographs generally show at least two roughly coplanar tracks. Within wide limits, all events showing just two outgoing particles, A and B, were measured to determine angles and intercepts of the tracks A and B as well as of the incoming pion

track, π. These measurements were then processed by a computer to select elastic events according to criteria of coplanarity, vertex fit, and agreement with elastic kinematics. If we let $\hat{\underline{\pi}}$, $\hat{\underline{A}}$, and $\hat{\underline{B}}$ be the unit vectors in the direction of motion in the laboratory of the incident pion, particle A, and particle B respectively, then the degree of coplanarity is defined by the angle ϕ where $\sin \phi = \hat{\underline{\pi}} \cdot (\hat{\underline{A}} \times \hat{\underline{B}}) / |\hat{\underline{A}} \times \hat{\underline{B}}|$. Given that Θ_A and Θ_B are defined from $\cos \Theta_A = \hat{\underline{\pi}} \cdot \hat{\underline{A}}$ and $\cos \Theta_B = \hat{\underline{\pi}} \cdot \hat{\underline{B}}$, the degree of conformity of Θ_A and Θ_B with a particular kinematic curve is measured by the distance D in degrees, defined as the perpendicular distance of the measured Θ_A-Θ_B point to the particular kinematics curve, as shown in Fig. 5.

Of course the precision of the angular measurements is limited by finite spark width, multiple scattering, optical distortions, etc., so that non-zero ranges of ϕ and D must be allowed. If these ranges are made too small, real two-body final-state events will be excluded. If these ranges are made too large, final-state events of three or more bodies may have too large a probability of acceptance. The elastic diffraction scattering has a large total cross section, several mb in this momentum range; and for these small angles the background-event contamination was negligible. Therefore the diffraction scattering data were used to determine the ranges of ϕ and D. We found that both ϕ and D fit a normal error curve with standard deviations of 0.4° and 0.6° respectively. These directly-measured standard deviations in ϕ and D agreed with those calculated from the standard deviations in the direct angular measurements. Calculations also showed that ϕ and D standard deviations were almost independent of Θ_A and Θ_B, and could be used in con-

siderations of large-angle elastic scattering when the background was important. Because of the loose criterion used in selecting events for measurement, events were obtained not only near the kinematics curves of interest but for a wide range of values of Θ_A and Θ_B. This gave a distribution of background events in the Θ_A-Θ_B plane which was found to vary slowly. If one considers an arbitrary line in the Θ_A-Θ_B plane, the background events which lie within one standard deviation in D of this line and are coplanar to within one standard deviation in ϕ yield an average background cross section of .004 mb/sr. This, then, determines the lower limit to detection of the differential elastic scattering cross section in the present experiment. As will be seen in Section IV, the large-angle scattering cross sections are very small, and this background is the principle source of the errors quoted.

The large-angle cross section was determined as follows. For a particular range of cos Θ along the π^- p kinematics curve, all events coplanar to one standard deviation in ϕ and within six standard deviations of D on both sides of the π^- p curve were collected. The events were distributed into equal intervals in D and a weighted least squares fit was made using the number of events in each D interval as the measured observable and D as the independent parameter to the equation of a linear background plus a gaussian distribution of elastic events around the kinematics curve. The errors were then increased over counting statistics by a factor proportional to the square root of $\chi^{2\ 24}$ for the fit as described above. This factor was typically between 1.0 and 1.5.

The data were corrected for the nuclear interactions and multiple scat-

tering of the recoil particles in the target, spark chambers, etc. The effective ϕ angle subtended by the coplanarity counters was evaluated as a function of θ_A and θ_B averaged over the target volume for the different θ_A and θ_B relationships for each incident beam momentum. The effective target length corresponding to the different scattering angles was also computed and used with the above factors to convert corrected numbers of elastic events to differential cross sections. The results and errors presented here for large-angle scattering differ from those reported earlier[1] primarily as a result of the explicit analysis subsequently performed.

The following data sample is drawn from over 50,000 photographs and corresponds to from 1500 to 1800 elastic events in each of the four data sets.

IV. RESULTS

The results are tabulated in terms of $d\sigma/d\Omega$(mb/sr) and $(d\sigma/d\Omega)/(k\sigma_t/4\pi)^2$ versus cos θ and t in Tables II through V. The errors given are statistical except for the large-angle points, where the statistical errors are scaled up somewhat, as discussed in Section III. In addition to the quoted statistical errors there is a normalization uncertainty in the π^- p data of $\pm 8\%$ and in the π^+ p data of possibly $^{+30}_{-10}\%$ (due to uncertainty in the proton contamination of the π^+ beam).

The data are plotted in Figs. 6 through 9 on a semilogarithmic scale versus t. The energy-independent exponential character of the diffraction peak is readily apparent. At 3 GeV/c there is some contribution to the

elastic cross sections out to rather large angles (large $|t|$). At 4 and 5 GeV/c, however, the cross section appears to fall to very low values in the backward hemisphere, and our data in this region permit only upper limits to be placed on the elastic cross section. In Fig. 10 the data are plotted with all negative pion points on one graph to emphasize the similarity in slopes of the diffraction peak. In Fig. 11, a log-log graph is presented with all four sets of data included for comparison with such theories as Serber's diffraction calculation.[10] It is apparent that the scatter in the data for $|t| > 1.0$ $(\text{GeV/c})^2$ precludes any statement concerning a fit to a power-law formula. Finally, the data do not show evidence of a backward peak (about 180°), although at 3 GeV/c a slight rise in the cross section behind 90° c.m. is not excluded.

V. DISCUSSION OF THE DIFFRACTION PEAK

A. Shape of the Diffraction Peak

From Figs. 6 through 9, or from Fig. 10 one can observe that the diffraction peak is at least roughly exponential for $|t|$ out to 0.8 $(\text{GeV/c})^2$. A purely exponential diffraction peak such as that predicted by the simplest Regge theory (Section II.B.3) would be described by

$$d\sigma/d\Omega = \exp[A_0+A_1 t] . \qquad (27)$$

The test of the exponential nature of the diffraction peak is made quantita-

tive in Table VI, where the parameters A_0 and A_1 of Eq. (27) are tabulated. These parameters were obtained by a weighted least squares fitting procedure. For later use, $(d\sigma/d\Omega)_0 = \exp[A_0]$ is also listed in Table VI. $P(\chi^2)$ is the probability of obtaining a larger χ^2 than the χ^2 value obtained in the particular fit. The observation of the exponential nature of the diffraction peak is confirmed for the interval $0 < |t| < 0.4$ $(GeV/c)^2$ for three of the sets of data; only the 3.15 GeV/c π^- p shows a low $P(\chi^2)$.

However, on extending the fits to values of $|t|$ up to 0.8 $(GeV/c)^2$ it is clear that the "tail" of the diffraction peak flattens out from (e.g., rises above) a purely exponential behavior. This is made more apparent from the values of A_1 fitted to the data in the interval $0.4 < |t| < 0.8$ and $0 < |t| < 0.8$, which are smaller than the values of A_1 fitted only to the data within the interval $0 < |t| < 0.4$. Thus the linear fit appears adequate for the latter range of $|t|$, but is not as satisfactory for the larger range of $|t|$. Only for the 4.95 GeV/c data is $P(\chi^2) > 0.01$ for the linear fit over the interval $0 < |t| < 0.8$.

By adding a quadratic term, the data can generally be fit much better over the larger range of $|t|$, so that in Table VII fitted quantities are listed for the equation

$$d\sigma/d\Omega = \exp[A_0+A_1t+A_2t^2) \ . \qquad (28)$$

Figures 12 through 15 display the data plotted only to $t = -1.4$ $(GeV/c)^2$, with the curves of Eq. (28) corresponding to values of the coefficients from Table VII [$0 < |t| < 0.8$ $(GeV/c)^2$] plotted for comparison.

While Eq. (28) is an empirical expression suggested by the discrepancies of Eq. (27), the plausibility of such an expression is also suggested by the arguments of Section II. Thus in the context of the simple Regge theory, $\alpha(t)$ may be non-linear, $\beta(t)$ may contain a dependence other than $\exp[\gamma t]$, or the contributions of other poles may modify the t-dependence as in Eq. (17).

From Tables VI and VII there appears to be little choice between Eqs. (27) and (28) in the interval $0 < |t| < 0.4$. However, the $P(\chi^2)$ is increased significantly for the 4.13 and 2.92 (GeV/c) data by including the t^2 term of Eq. (28) over the interval $0 < |t| < 0.8$.

The consistently poor fit of the 3.15 GeV/c data to Eqs. (27) and (28) is not understood. Unless a systematic error entered into the data, either there is an unusual statistical fluctuation in some data points or the physics at this energy is basically different. Comparison of the data curves and the A parameters reveals that the 3.15 GeV/c data is at least qualitatively similar to the other data.

Average values of A_1 and A_2 can be found by taking the values of the A parameters for Eq. (28) fitted over the interval $0 < |t| < 0.8$ as the most significant, and by noting that there are no significant differences between the data or the values of A_1. The average value of A_1 for the four curves is 9.6 $(\text{GeV/c})^{-2}$, and that of A_2 is 3.3 $(\text{GeV/c})^{-4}$. Since the $P(\chi^2)$ of obtaining the experimental values of A_1 and A_2 from these average values is 0.05 and 0.02 respectively, we cannot say that all the curves are characterized by the same A_1 and A_2. But we can use these average values for com-

parison with the average A_1 of 7.9 $(\mathrm{GeV/c})^{-2}$ obtained from Table VI for the interval $0 < |t| < 0.4$. These two averaged fits give

$$0 < |t| < 0.4\ (\mathrm{GeV/c})^2; \quad \left(\frac{d\sigma}{d\Omega}\right) = \left(\frac{d\sigma}{d\Omega}\right)_0 \exp[7.9t] \ ,$$
$$0 < |t| < 0.8\ (\mathrm{GeV/c})^2; \quad \left(\frac{d\sigma}{d\Omega}\right) = \left(\frac{d\sigma}{d\Omega}\right)_0 \exp[9.6t + 3.3t^2] \ , \tag{29}$$

which serves to emphasize further that there is a substantial deviation from the simple exponential when $|t|$ is extended to 0.8 $(\mathrm{GeV/c})^2$.

Of course the quadratic terms may still be important at smaller $|t|$; our measurements do not go to small enough angles to allow exploration of this possibility.

B. The Forward Scattering Cross Section

Table VIII lists the square of the imaginary part of the forward scattering amplitude, $(k\sigma_{tot}/4\pi)^2$, and the forward scattering cross sections $(d\sigma/d\Omega)_0$ obtained by the various fitting methods of Section V.A. The errors given with the $(d\sigma/d\Omega)_0$ quantities are derived from the least squares fitting procedure. At each energy an estimated overall normalization uncertainty is also listed. For the π^+ p data this error is large and precludes any meaningful comparison. The ratio $\mathcal{R} = (d\sigma/d\Omega)_0/(k\sigma_{tot}/4\pi)^2$ include the errors on each quantity and the normalization error.

First we observe that the $(d\sigma/d\Omega)_0$ values at a particular energy vary according to the fitting method, the "quadratic" fits usually giving a higher value than the "linear" fit. Considering just the π^- p data we next observe

that in eight out of nine cases the ratio $\mathcal{R} = (d\sigma/d\Omega)_0/(k\sigma_{tot}/4\pi)^2$ is greater than 1.00, indicating a real part to the forward scattering amplitude. Of course in each case the error is such as to allow the ratio to be 1.00. A weighted average over the data and over the three fitting methods results in the following values for the ratio $\mathcal{R}$:

$$\mathcal{R} = 1.20 \pm .05 \text{ for } 4.13 \text{ and } 4.95 \text{ data combined}$$

$$\mathcal{R} = 1.12 \pm .04 \text{ for all } \pi^- p \text{ data.}$$

Therefore if the differential cross section behaves as an exponential in t for small $|t|$, the $|\text{Re } f(0)|^2/|\text{Im } f(0)|^2$ may be about 0.1 to 0.2 in this energy range. In order for the $|\text{Re } f(0)|^2$ to be smaller, the differential cross section must flatten out a little for very small $|t|$.

If the method of Cronin[25] is followed, so that single integral dispersion relations are used to calculate the value of $[\text{Re } f(0)]^2$, one finds that the $[\text{Re } f(0)]^2$ averaged over this momentum range is about 0.5 mb. As this yields $\mathcal{R} \cong 1.017$, the measured $\mathcal{R} = 1.12 \pm .04$ is too high by 2.5 standard deviations.

This can be interpreted in three ways. First, the normalization of the data may be wrong. Second, the exponential from, and particularly the use of the quadratic term, may be wrong for very small $|t|$. Thus the linear exponent gives an average $\mathcal{R}$ of $1.09 \pm .06$, which is lower than the average $\mathcal{R}$ obtained when all the fitting methods are used. The third interpretation is that the forward dispersion relations are wrong, but this involves such a fundamental relationship in field theory that much stronger evidence would be required than is presented here. Therefore our preference for an explanation

goes first to a systematic error in the normalization of the differential cross section and second to the possibility of an incorrect form having been used for $d\sigma/d\Omega$ at very small $|t|$.

It may be noted that the ratio $\mathcal{R}$ appears, from the data presented here, to increase monotonically with incident pion energy. This same trend is consistent with the value of $\mathcal{R}$ determined in preliminary analysis of 2 GeV/c π^- p data taken at the same time as these data and this trend is also consistent with the results of Brandt et al.[8]

C. The Total Elastic Cross Section

In Table IX we present the total elastic cross section according to the various fitting methods used to extrapolate the data to small angles. In each case the elastic cross section is evaluated from the experimental data points for all values of t greater than the minimum observable. The fitted curves are used only to estimate the cross section between these minimum measured points and the point t = 0. We have also included in Table IX an elastic cross section based on extrapolation to the optical theorem point at t = 0.

As a result of more careful normalization, extrapolation, and background subtraction, the elastic cross sections of Table IX average a few percent lower than the preliminary values given earlier. The total cross sections given are from the smooth curve of Diddens et al.[26] These values average slightly higher than the ones obtained earlier;[27] consequently the ratios of elastic to total cross sections (averaging about 20% for the π^- data) appear

to be in somewhat closer agreement with the optical model proposed by Serber[10] (0.185 for $\eta = 1$) than was indicated earlier. But from Table IX it is clear that in addition to normalization uncertainties, the exact value of the total elastic cross section is sensitive to the manner in which we extrapolate to $t = 0$. These data must be interpreted accordingly.

D. The Simple Optical Model Fit to the Diffraction Peak

The forward part of the diffraction peak was used to evaluate R and (1-a) in the simple optical model for a partially absorbing nucleus. A weighted least squares fit was used to evaluate R from the equation

$$\frac{d\sigma}{d\Omega}(\theta) = \frac{k^2 \sigma_{tot}^2}{16\pi^2} 4 \left[\frac{J_1(kR \sin\theta)}{kR \sin\theta} \right] .$$

Then the quantity (1-a) was found from the equation

$$\sigma_{tot} = 2\pi(1-a)R^2 .$$

The results are given in Table X. The maximum kR sin θ used was about 3.0, corresponding to $|t|$ of about 0.3 to 0.4 $(GeV/c)^2$. Only the most forward points were used because the simple optical model with a uniform opacity drops below the experimental points for larger angles, making it impossible to get any meaningful fit. For example, if at 2.92 GeV/c the next two points are also used to obtain a value for kR, the kR changes from 6.25 to 6.1 and the minimum χ^2 increases from 8.4 to 17.0. As there are three degrees of freedom, this corresponds to a much worse fit.

The values of R are quite similar to those found at some other momenta in π^- p elastic scattering. Thus at 1.43 GeV/c, R = 1.08×10^{-13} has been reported;[28] and at 5.17 GeV/c, R = 1.04×10^{-13} has been reported.[29] Our average value for R for the π^- p system is $(1.04 \pm .03) \times 10^{-13}$ cm. The probability of these values having come from the same true value is 20%.

The optical model prediction of Serber[10] cannot be tested easily by our differential cross section data; the statistical accuracy of the data for $|t| > 1.0$ $(\text{GeV/c})^2$ is poor, and it is only for these large $|t|$ values that significant deviations between an exponential and a power law fit can be expected. Yet our data are sufficient to demonstrate that the differential cross sections for large $|t|$ fall more rapidly for 4 and 5 GeV/c than for 3 GeV/c scattering. This is in disagreement with an optical model containing no energy dependence. All the π^- data are plotted in Fig. 11 on a log-log scale.

E. The Variation of the Diffraction Peak Width and Shape With Energy

While the simplest application of the Regge theory to the diffraction peak through Eq. (19) may be inapplicable in principle, the exponential shape of the peak allows one to use the parameterization of Eq. (20) as a rough test of the variation of the diffraction peak width with energy. In a previous paper[1] A_1 was taken from our data and other published results, and it was shown that there was no statistically significant evidence for a charge

of A_1 with energy (specifically with ℓns) from 3 to 16 GeV. The same conclusion holds for all the fits we have tried. We find no systematic change in the various sets of exponential parameters with s and specifically we see no shrinkage of the diffraction peak for small $|t|$. We may now compare our average A_1 of 8.0 ± 0.2 $(\text{GeV/c})^{-2}$ for the $0.0 < |t| < 0.4$ (GeV/c) interval with the recent measurements of Foley et al.,[2] of π^- p elastic scattering in the 7 to 17 GeV/c region and with the measurements of Brandt et al.,[8] at 10 GeV/c. Over the $|t|$ interval 0.2 to 0.4 $(\text{GeV/c})^2$ the Brookhaven published graphical data yield $A_1 \cong 7.7$ $(\text{GeV/c})^{-2}$, and the Brandt data yield $A_1 = 7.5\pm0.3$ $(\text{GeV/c})^2$. The excellent agreement demonstrates that the statement of no shrinkage made by Foley et al., can be extended down to 3.0 GeV/c. The constancy of A_1 over this entire energy range is rather remarkable.

Our three-parameter fit over the interval $0 < |t| < 0.4$ $(\text{GeV/c})^2$ yields average values of $A_1 = 8.9\pm1.0$ and $A_2 = 1.2\pm1.8$; over the interval $0 < |t| < 0.8$ $(\text{GeV/c})^2$ it yields $A_1 = 9.6\pm0.4$ and $A_2 = 3.3\pm0.5$. For this same interval at 10 GeV/c, Brandt et al., gives $A_1 = 11.4\pm1.07$ and $A_2 = 8.9\pm2.8$. Since these 10-GeV/c parameters are different from both sets of ours, there seems to be a definite change of shape of the diffraction peak over the 3 to 10 GeV/c region, although the average slope (using just a two-parameter fit) does not change over this energy interval. While some of the difference between the quadratic coefficients at 5 and 10 GeV/c may be due to the data for very small $|t|$ at 10 GeV/c, the deviations from an exponential fit between the two sets of data at large $|t|$ appear significant.

The original shrinkage concept in the Regge theory came from the energy dependence of the linear term in the exponent as shown in Eq. (20). In an attempt to find a more subtle type of energy dependence we can write a generalization of Eq. (20), i.e., an expansion of Eq. (18) as follows:

$$\frac{d\sigma}{dt} = \left(\frac{d\sigma}{dt}\right)_{t=0} \exp[(\gamma_1 t+\gamma_2 t^2+ \ldots) + 2(\alpha_1 t+\alpha_2 t^2+ \ldots)\ell ns] . \quad (30)$$

Now there is no evidence for $\alpha_1 \neq 0$ in π^- p elastic scattering and yet it is strongly intuited that the slope of the Pomeranchuk trajectory at t = 0, $(d\alpha(t)/dt)_{t=0}$, should be positive.[14] According to this idea, therefore, if $\alpha_1 = 0$, α_2 should also be quite small and the first substantial α term would be α_3, reducing Eq. (30) to

$$\frac{d\sigma}{dt} = \left(\frac{d\sigma}{dt}\right)_0 \exp[(\gamma_1 t+\gamma_2 t^2+ \ldots) + 2\alpha_3 t^3 \ell ns] . \quad (31)$$

To see if Eq. (31) might be applicable, the data have been fitted to

$$\frac{d\sigma}{dt} = \exp[A_0+A_1 t+A_3 t^3] \quad (32)$$

over the interval $0 < |t| < 0.8$ $(GeV/c)^2$. The t^2 term was left out so that the statistical uncertainty in the A_3 term would not be too large. The parameters are given in Table VII. The result is similar to the quadratic fit in that there is no major change in the $P(\chi^2)$; and the 4.95 (GeV/c) A_3 is smaller than the lower-momentum A_3 values just as the 4.95 (GeV/c) A_2 is smaller than the lower-momentum A_2 values. Thus there is no evidence either for or against the use of the $A_3 t^3$ term instead of the $A_2 t^2$ term.

F. The Diffraction Peak and Large-Angle Scattering as a General Function of s and t

In this section we shall treat more than the diffraction peak in order to see how all $d\sigma/d\Omega$ behaves as a general function of s and t. First the results are presented in graphical form in Fig. 16, which goes out to values of $|t| \lesssim 2(\text{GeV/c})^2$. At this $|t|$ the data change from giving a value for the cross section to giving primarily upper limits. In Fig. 15, $(4\pi/k\sigma_{tot})^2$ $(d\sigma/d\Omega)$, which we shall refer to as the normalized differential cross section, is plotted versus s for various values of t. The errors include the statistical error from each measured point propagated through the interpolation process and the normalization error, which is equivalent to an uncertainty in $(d\sigma/d\Omega)$. At $t = -0.1$, -0.3, -0.5, and -0.7 $(\text{GeV/c})^2$ there is generally a slight rise in the normalized differential cross section with increasing s. As discussed in Section V.B, this same effect produces an increasing ratio of the extrapolated $(d\sigma/d\Omega)_0$ to the optical theorem $(d\sigma/d\Omega)_0$ and can easily be due to an energy-dependent error in the normalization. If the normalization is correct, then this effect is a slight broadening of the diffraction peak <u>without</u> a change in the slope. By taking forward scattering dispersion theory as correct, one implies that the shape of the differential cross section at very small $|t|$ is changing throughout the region.

For $t = -1.0$ and -2.0 $(\text{GeV/c})^2$ the normalized differential cross section is clearly decreasing with s. At $t = -1.0$ it decreases by a factor of 2 in s, going from 6.8 to 10.2 $(\text{GeV/c})^2$; and at $t = -2.0$ it decreases by a factor of about 5 over the same interval.

For another means of studying the entire differential cross section as a function of s and t, we have made a weighted least square fit for the entire range of $|t|$ to the equation

$$\frac{d\sigma}{d\Omega} = \exp[A_0+A_1t+A_2t^2+A_3t^3+A_4t^4] .$$

The results are presented in Table XI. Except for the 3.15 GeV/c data the equation is a fair fit. In contrast, Eqs. (28) and (32), which use only three parameters, are very bad fits in all cases. Comparing the different sets of data, one finds as before that the A parameters are roughly the same for all the data, but that the spread is outside statistics. In particular we observe that

$$A_1 > A_2 > A_3 > A_4 ,$$

so that for $|t| < 1$ $(GeV/c)^2$ we can think of this as a converging expansion of some function of t. Although we have produced a reasonable fit to all the data out to large $|t|$ values, present theory provides no way to interpret the parameters. At most, one can say that these parameters are certainly allowable in more complex forms of the Regge theory.

In comparing the graphical and parametric methods of examining the general s- and t-dependence it is interesting to note that as the incident pion momentum increases from 3.15 to 4.95 GeV/c, A_2, A_3, and A_4 all decrease. Now for $|t| > 1.0$ $(GeV/c)^2$ these are the important parameters; consequently the large $|t|$ value scattering will tend to decrease as s increases, as is apparent in Fig. 15. In addition, the parametric fits demonstrate that the decrease

in the cross section with increasing energy is probably not due to a chance cancellation of the odd and even powers of t in the exponential, but rather to a decrease in all terms.

VI. DISCUSSION OF LARGE-ANGLE SCATTERING

A. Shape of the Large-Angle Differential Cross Section and Existence of a Backward Peak

From the tables and graphs already presented it is clear that the general character of the differential cross sections is a roughly exponential drop to 1 or 2 $(\mathrm{GeV/c})^2$ four-momentum transfer, with the cross section at larger $|t|$ either flattening or (at higher energies) continuing to fall. At 4.13 and 4.95 (GeV/c) our data primarily represent upper limits for $|t| > 2$ $(\mathrm{GeV/c})^2$. Thus our entire data can be represented in terms of t-channel processes through more complex application of Regge theory or through some alternative. In particular, it does not appear necessary to invoke u-channel processes (e.g., baryon exchange) in order to interpret this experiment.

We may use our upper limits to the cross section at large angles to set limits to the width or height of a possible backward peak in the differential cross section. Our data extend only to $\cos\theta = -0.93$ and are sensitive to a differential cross section of the order of 5×10^{-3} mb/sr. The limits placed on large-angle scattering by the present data and by other published data are summarized in Table XII, where $d\sigma/d\Omega$ for $0 > \cos\theta > -1.0$, $d\sigma/d\Omega$ for the

backward steradian, and the maximum observed angle (center of mass) from each experiment are tabulated. As an example, one may postulate a backward peak which has the same width as the forward diffraction peak and is given by

$$\frac{d\sigma}{d\Omega} = \exp[A_0 + A_1(u-u_0)] ,$$

where u_0 is the value of u at 180° and the differential cross section is a function of $\theta' = 180°-\theta$. Our data indicate that in this case a backward peak at 4.13 GeV/c would have to be less than 1/24 the height of the forward peak.

The broader peak suggested by Singh and Udgaonkar[20] from the strip approximation is more strongly limited by the data, but the slightly narrower peak obtained by the optical model approximation applied to 180° (see Section II and the Appendix) is not as strongly limited, in view of the maximum angles observed in this experiment. Our data suggest that such a peak would have to be less than 10% of the forward peak. As stated in Section II, neither the virtual nucleon and nucleon isobar exchange theory nor the Regge theory of the backward peak give a width prediction, so we cannot set a limit on those particular theoretical predictions.

The bubble chamber measurements (which do extend to 180°) in π^- p set limits of 30 μb/sr and in π^+ p set limits of 14 to 90 μb/sr over our energy range; these limits are consistent with our data. Since the diffraction peak is completely contained in the first steradian in this energy range and totals about 6 mb, the total elastic cross section in any backward peak is, roughly, less than 1/200 of the total elastic cross section for π^- p and less than 1/70 for π^+ p. Therefore, in comparison with the forward peak, the height

of the backward peak is either very small or its width is very narrow. The only data on this point come from the experiment on π^+ p by Kulakov et al.[30] using counters at 3.14 and 4.6 GeV/c. At 180° they found $d\sigma/d\Omega$ of 0.92±0.47 and 0.38±0.24 mb/sr.

This experiment only measured $d\sigma/d\Omega$ over a solid angle of 0.002 steradians about 180° in the center of mass. From other measurements listed in Table XII it is highly probable that the total backward elastic peak is less than 30 mb. To reconcile these two numbers one must postulate a very narrow backward peak, mostly lying behind cos θ = -0.985 to -0.995.

The theoretical interpretation of such a peak is obscure. It is too narrow to be explained by the backward peak arising from the optical model. It is also too narrow to be treated with present Regge theory, because it lies in the region shown by Table I to correspond to small cos θ_u. It is too small for the simple nucleon exchange calculation given by Cook et al.,[7] although it may fit the unpublished calculation of Pomeranchuk.

It would seem wise to wait for further experimental education of this peak before developing the theory further. The measurement of large-angle elastic scattering at these high energies is made difficult by the problem of inelastic contamination, and the counter technique employed by Kulakov et al.,[30] seems particularly subject to this kind of error.

B. Energy Dependence of the Large-Angle Scattering

On the basis of the data in Table XII, only qualitative statements can be made regarding the energy dependence of the elastic cross sections in the

backward hemisphere. Below 2.5 GeV/c pion momentum, the existence of resonances in the total pion-nucleon cross section has been established; these resonances are probably the most important determinants of magnitude and shape for the large-angle cross sections near the resonance energies.

The statistical model[18] makes no predictions about the angular distributions of the elastic scattering through this channel except that any distribution should be symmetric about 90° c.m. The energy dependence of large-angle scattering predicted by the statistical model is an exponential multiplied by a factor such as s^{-1} to give the probability of forming an intermediate state. From the Regge theory of the t-channel, the $\alpha(t)$ for all Regge trajectories should approach -1 for sufficiently negative t. This would give rise to a differential cross section at large $|t|$ such that $d\sigma/d\Omega \propto s^{-4}$ in this region. The data at 3 GeV/c and the upper limits given for the higher energies are consistent with either prediction, e.g., that the cross section in the backward hemisphere falls rapidly to very low values with increasing energy.

VII. COMPARISON OF PION-PROTON WITH PROTON-PROTON ELASTIC SCATTERING

Qualitatively, the p p differential elastic scattering resembles the $\pi^{\pm}$ p data presented above. A detailed comparison, however, reveals significant differences between the two processes. Available p p data in the same energy range as our π p data have been fit in the same manner as the π p data. In Table XIII, the coefficients for the fit

$$\frac{d\sigma}{d\Omega} = \exp[A_0 + A_1 t]; \quad 0 \leq |t| \leq 0.4 \ (\text{GeV/c})^2 \qquad (33)$$

and

$$\frac{d\sigma}{d\Omega} = \exp[A_0 + A_1 t + A_2 t^2]; \quad 0 \leq |t| \leq 0.8 \ (\text{GeV/c})^2 \qquad (34)$$

are given for the p p data. Figure 17 compares A_1 for the two processes (from the linear fit) versus s, where straight lines of the form $A_1 = C_1 + C_2 \ell n s$ have been fit to the p p data and to the π^- p data. A clear increase of A_1 with s is evident for the p p data, such that A_1 would have the same value for π^- p and for p p scattering at s of about 16 $(\text{GeV})^2$. In Fig. 17 data fit to π^- p scattering experiments at lower energies are also included where the corresponding fitted quantities are given in Table XIV.

The π^- p and p p diffraction peaks can also be compared by using the "quadratic" fit of Eq. (34). Table XV presents the average values of A_1 and A_2 for p p and π^- p over the s range 6 to 12 $(\text{GeV})^2$. The quadratic fits to $|t| = 0.8 \ (\text{GeV/c})^2$ again demonstrate the narrower $\pi^\mp$ p diffraction peak, although there is no significant difference in A_2 values between the two processes. When the entire angular range is considered, however, further significant differences in shape appear. In Fig. 18 the normalized differential cross sections of all the present $\pi^\pm$ p data for $|t| > 0.4 \ (\text{GeV/c})^2$ are plotted together with smooth curves for the p p scattering at s = 7.5 and 11.8 $(\text{GeV})^2$. For $|t| > 1.0 \ (\text{GeV/c})^2$, the $\pi^\pm$ p elastic cross section appears consistently to be several times smaller than the corresponding p p.

It is thus clear that π^- p and p p elastic scattering behave quite differently in this region of energy.

ACKNOWLEDGMENTS

We wish to acknowledge the gracious hospitality, interest, and enthusiastic support of Dr. E. M. McMillan, Dr. E. J. Lofgren, and the staff of the Bevatron of the Lawrence Radiation Laboratory. We are deeply indebted to Dr. K. W. Lai and Dr. D. E. Damouth for considerable assistance in the design and execution of some aspects of this experiment. We would also like to thank R.Y.Y. Lee, O. Haas, and our capable group of scanners for their contributions.

APPENDIX

We will derive formulas for the forward and backward peaks for the simplest type of optical model. From (6) and (7)

$$f(\theta) = \left(\frac{1-a}{2ik}\right) \sum_{\ell=0}^{L} (2\ell+1) \mathcal{P}_\ell(\cos\theta) \ . \tag{A1}$$

Then

$$f(\theta) = \left(\frac{1-a}{2ik}\right) [\mathcal{P}'_{L+1}(\cos\theta) + \mathcal{P}'_L(\cos\theta)] \ . \tag{A2}$$

For θ close to 0°, $\cos\theta \cong 1-(\theta^2/2)$, so that for forward scattering $\cos\theta$ is replaced by $1-(\theta^2/2)$ in (A2).

For θ close to 180° let $\theta' = 180°-\theta$, so that θ' is small. Then

$$\cos\theta \cong -\left(1 - \frac{\theta'^2}{2}\right).$$

For the backward scattering (A2) then becomes

$$\begin{aligned} f(\theta') &= \left(\frac{1-a}{2ik}\right)\left\{\mathcal{P}'_{L+1}\left(-\left[1 - \frac{\theta'^2}{2}\right]\right) + \mathcal{P}'_L\left(-\left[1 - \frac{\theta'^2}{2}\right]\right)\right\} \\ &= \left(\frac{1-a}{2ik}\right)(-1)^L\left[\mathcal{P}'_{L+1}\left(1 - \frac{\theta'^2}{2}\right) - \mathcal{P}'_L\left(1 - \frac{\theta'^2}{2}\right)\right] \ . \end{aligned} \tag{A3}$$

Now, letting x be $[1-(\theta^2/2)]$ in (A2) and $[1-(\theta'^2/2)]$ in (A3), we note that

$$\mathcal{P}'_L(x) = \frac{(L+1)!}{2(L-1)!}\left[1 - \frac{(L-1)(L+2)}{(1)(2)}\left(\frac{1-x}{2}\right) + \frac{(L-1)(L-2)(L+2)(L+3)}{(1)(2)(2)(3)}\left(\frac{1-x}{2}\right)^2\right.$$

$$\left. - \frac{(L-1)(L-2)(L-3)(L+2)(L+3)(L+4)}{(1)(2)(3)(2)(3)(4)}\left(\frac{1-x}{2}\right)^3 + \ldots\right] \ .$$

Then

$$\mathcal{P}'_{L+1}(x) \pm \mathcal{P}'_{L}(x) = \frac{(L+1)!}{2(L-1)!}\left[\left(\frac{L+2}{L} \pm 1\right) - \left(\frac{(L+2)(L+3)}{2} \pm \frac{(L-1)(L+2)}{2}\right)\left(\frac{1-x}{2}\right)\right.$$
$$+ \left(\frac{(L+2)(L-1)(L+3)(L+4)}{12} \pm \frac{(L-1)(L-2)(L+2)(L+3)}{12}\right)\left(\frac{1-x}{2}\right)^2$$
$$- \left(\frac{(L+2)(L-1)(L-2)(L+3)(L+4)(L+5)}{144} \pm \frac{(L-1)(L-2)(L-3)(L+2)(L+3)(L+4)}{144}\right)$$
$$\left.\left(\frac{1-x}{2}\right)^3 + \ldots\ldots\right] .$$

Thus

$$\mathcal{P}'_{L+1}(x) + \mathcal{P}'_{L}(x) = \frac{(L+1)!}{2(L-1)!}\left[\left(2 + \frac{2}{L}\right) - \frac{1}{2}(L+2)(2L+2)\left(\frac{1-x}{2}\right)\right.$$
$$+ \frac{1}{12}(L+2)(L-1)(L+3)(2L+2)\left(\frac{1-x}{2}\right)^2$$
$$\left. - \frac{1}{144}(L+2)(L-1)(L-2)(L+3)(L+4)(2L+2)\left(\frac{1-x}{2}\right)^3 + \ldots\right] ,$$

whereas

$$\mathcal{P}'_{L+1}(x) - \mathcal{P}'_{L}(x) = \frac{(L+1)!}{2(L-1)!}\left[\frac{2}{L} - \frac{1}{2}(L+2)(4)\left(\frac{1-x}{2}\right)\right.$$
$$+ \frac{1}{12}(L+2)(L-1)(L+3)(6)\left(\frac{1-x}{2}\right)^2$$
$$\left. + \frac{1}{144}(L+2)(L-2)(L-2)(L+3)(L+4)(8)\left(\frac{1-x}{2}\right)^3 + \ldots\right] .$$

Now we set $L \gg 1$ and replace x by $1-(\theta^2/2)$ or $1-(\theta'^2/2)$.

Then

$$\mathcal{P}'_{L+1}(x) + \mathcal{P}'_{L}(x) = L^2\left[1 - \frac{L^2\theta^2}{(2)(4)} + \frac{L^4\theta^4}{(12)(16)} - \frac{L^6}{(144)(64)} + \ldots\right] , \quad (A4)$$

and

$$\mathcal{P}'_{L+1}(x) - \mathcal{P}'_{L}(x) = L\left[1 - \frac{L^2\theta'^2}{4} + \frac{L^4\theta'^4}{(4)(16)} - \frac{L^6\theta'^6}{(36)(63)} + \ldots\right] . \quad (A5)$$

Now

$$J_1(x) = \frac{x}{2}\left[1 - \frac{x^2}{(2)(4)} + \frac{x^4}{(12)(16)} - \ldots\right] . \quad (A6)$$

By setting $L\theta = kR\theta$ and using (A6), (A4), and (A2),

$$f(\theta) = \left(\frac{1-a}{2ik}\right)\left(\frac{2kR}{\theta}\right) J_1(kR\theta) .$$

The forward diffraction peak differential cross section is therefore

$$\frac{d\sigma}{d\Omega} = (1-a)^2R^2/\theta^2\,[J_1(kR\theta)]^2$$

$$= (1-a)^2k^2R^4\left[\frac{J_1(kR\theta)}{kR\theta}\right]^2 .$$

Similarly, setting $L\theta' = kR\theta'$ and using (A5) and (A3),

$$f(\theta') = \left(\frac{1-a}{2ik}\right)(-1)^L(kR)\left[1 - \frac{(kR\theta'/2)^2}{1^2} + \frac{(kR\theta'/2)^4}{(2!)^2} - \frac{(kR\theta'/2)^6}{(3!)^2} + \ldots\right] .$$

We define

$$B(kR\theta') = \frac{1}{2}\left[1 - \frac{(kR\theta'/2)^2}{(1!)^2} + \ldots\right] .$$

Then the backward peak is given by

$$d\sigma/d\Omega_{backward} = (1-a)^2R^2[B(kR\theta')]^2 .$$

REFERENCES

1. C. C. Ting, L. W. Jones, and M. L. Perl, Phys. Rev. Letters 9, 468 (1962).
2. K. J. Foley et al., Phys. Rev. Letters 10, 376 (1963).
3. L. W. Jones et al., Proceedings of the 1962 International Conference on High-Energy Physics at CERN (CERN, Geneva, 1962), p. 591.
4. A. N. Diddens et al., Phys. Rev. Letters 9, 108 (1962).
5. B. Cork, W. A. Wenzel, and C. W. Causey, Jr., Phys. Rev. 107, 859 (1957).
6. Y. Goldschmidt-Clermont et al., CERN/TC/Physics, 62-5 (unpublished).
7. V. Cook et al., Phys. Rev. 129, 2743 (1963).
8. S. Brandt et al., Phys. Rev. Letters 10, 413 (1963).
9. I. Pomeranchuk, Soviet Phys.—JETP 7, 499 (1958).
   V. S. Barashenkov, Soviet Phys.—Uspekhi 3, 689 (1961).
10. R. Serber, Phys. Rev. Letters 10, 357 (1963).
11. G. F. Chew, S-Matrix Theory of Strong Interactions (W. A. Benjamin, New York, 1961).
12. D. Amati, S. Fubini, and A. Stanghellini, Phys. Rev. Letters 1, 29 (1962).
    D. Amati et al., Nuovo Cimento 22, 569 (1962).
13. C. Lovelace, Nuovo Cimento 25, 730 (1962).
14. G. F. Chew and S. C. Frautschi, Phys. Rev. Letters 7, 394 (1961).
15. S. C. Frautschi, M. Gell-Mann, and F. Zachariasen, Phys. Rev. 126, 2204 (1962).

16. S. D. Drell, Proceedings of the 1962 International Conference on High-Energy Physics at CERN (CERN, Geneva, 1962), p. 897.

17. F. Hadjioannou, R.J.N. Phillips, and W. Rarita, Phys. Rev. Letters 9, 183 (1962).

18. G. Fast and R. Hagedorn, Nuovo Cimento 27, 208 (1963).

G. Fast, R. Hagedorn, and L. W. Jones, Nuovo Cimento 27, 856 (1963).

19. D. I. Blokhintsev, Nuovo Cimento 23, 1061 (1962).

20. V. Singh and B. M. Udgaonkar, Phys. Rev. 123, 1487 (1961).

21. V. Cook et al., Phys. Rev. 130, 762 (1963).

22. Y. D. Boyukov et al., Soviet Phys.—JETP 14, 40 (1962).

23. The apparatus and technique of this experiment are further discussed in E. Bleuler et al., Nuclear Inst. and Methods 20, 208 (1963).

24. P. Cziffra and M. J. Moravscik, UCRL Report 8523 (1958) (unpublished).

25. J. W. Cronin, Phys. Rev. 118, 824 (1960).

26. A. N. Diddens et al., Phys. Rev. Letters 10, 262 (1963).

27. M. J. Longo and B. J. Moyer, Phys. Rev. Letters 9, 466 (1962).

28. M. Chretien et al., Phys. Rev. 108, 383 (1957).

29. R. G. Thomas, Phys. Rev. 120, 1015 (1960).

30. B. A. Kulakov et al., Proceedings of the 1962 International Conference on High-Energy Physics at CERN (CERN, Geneva, 1962), p. 584.

Table I

Cos θ at 4.0 GeV/c and 10.0 GeV/c in π p Elastic Scattering for Particular Values of Cos θ_u

Cos θ_u	4.0 GeV/c π p		10.0 GeV/c π p	
	Cos θ	θ	Cos θ	θ
- 1.0	-1.000	180°	-1.000	180°
+ 1.0	-0.974	167°	-0.992	173°
+ 3.0	-0.925	158°	-0.987	171°
+10.0	cannot be reached		-0.941	160°

Table II

Elastic Scattering Differential Cross Sections for 2.92 GeV/c

$\pi^+ p$; $s = 6.38\ (\mathrm{GeV})^2$, $\ell n\ s = 1.85$

Cos θ	$\frac{d\sigma}{d\Omega}$ $\frac{mb}{sr}$	$-t\left[\frac{GeV}{c}\right]^2$ at Center of Interval	$-u\left[\frac{GeV}{c}\right]^2$ at Center of Interval	$\left[\frac{4\pi}{k\ \sigma_{tot}}\right]^2 \frac{d\sigma}{d\Omega}$
0.97 to 0.96	7.33 ±0.64	0.082		0.4654±0.0406
0.96 to 0.94	4.80 ±0.33	0.118		0.3043±0.0210
0.94 to 0.92	3.81 ±0.29	0.164		0.2419±0.0184
0.92 to 0.90	2.30 ±0.21	0.212		0.1460±0.0133
0.90 to 0.88	1.62 ±0.18	0.258		0.1028±0.0114
0.88 to 0.86	1.03 ±0.13	0.306		0.0654±0.0082
0.86 to 0.84	0.87 ±0.13	0.352		0.0552±0.0082
0.84 to 0.82	0.71 ±0.12	0.400		0.0451±0.0076
0.82 to 0.80	0.53 ±0.11	0.446		0.0336±0.0070
0.80 to 0.78	0.39 ±0.09	0.494		0.0248±0.0057
0.78 to 0.76	0.43 +0.10	0.540		0.0273±0.0063
0.76 to 0.74	0.27 ±0.08	0.588		0.0171±0.0051
0.74 to 0.62	0.086±0.022	0.752		0.0055±0.0014
0.62 to 0.49	0.016±0.014	1.05	3.54	0.0010±0.00089
0.49 to -0.24	0.023±0.012	2.06	2.53	0.0015±0.00076
-0.24 to -0.46	0.035±0.021	3.17	1.41	0.0022±0.0013
-0.58 to -0.92	0.004±0.004	4.11	0.474	0.0002±0.0002

Table III

Elastic Scattering Differential Cross Sections for 3.15 GeV/c

$\pi^- p$; $s = 6.81(\text{GeV})^2$, $\ell n\ s = 1.92$

Cos θ	$\frac{d\sigma}{d\Omega}$ mb/sr	$-t\left[\frac{\text{GeV}}{c}\right]^2$ at Center of Interval	$-u\left[\frac{\text{GeV}}{c}\right]^2$ at Center of Interval	$\left[\frac{4\pi}{k\ \sigma_{tot}}\right]^2 \frac{d\sigma}{d\Omega}$
0.97 to 0.96	9.30 ±0.64	0.090		0.4554 ±0.0313
0.96 to 0.94	6.15 ±0.34	0.128		0.3012 ±0.0166
0.94 to 0.92	4.99 ±0.29	0.179		0.2444 ±0.0142
0.92 to 0.90	3.15 ±0.23	0.231		0.1543 ±0.0113
0.90 to 0.88	2.08 ±0.19	0.282		0.1019 ±0.0093
0.88 to 0.86	0.96 ±0.11	0.333		0.0470 ±0.0054
0.86 to 0.84	0.64 ±0.11	0.384		0.0313 ±0.0054
0.84 to 0.82	0.45 ±0.09	0.436		0.0220 ±0.0044
0.82 to 0.80	0.48 ±0.09	0.487		0.0235 ±0.0044
0.80 to 0.78	0.26 ±0.07	0.538		0.0127 ±0.0034
0.78 to 0.76	0.31 ±0.08	0.589		0.0152 ±0.0039
0.76 to 0.66	0.069±0.022	0.743		0.0034 ±0.0011
0.66 to 0.56	0.036±0.019	0.999		0.0018 ±0.00093
0.56 to 0.37	0.036±0.017	1.37	3.65	0.0018 ±0.00083
0.37 to -0.13	0.019±0.010	2.25	2.76	0.00093±0.00049
-0.13 to -0.47	$^{+0.007}_{0.000}$	3.33	1.69	$0.00000^{+0.00034}_{-0.00000}$
-0.47 to -0.92	$0.003^{+0.003}_{-0.003}$	4.34	0.674	$0.00015^{+0.00015}_{-0.00015}$

Table IV

Elastic Scattering Differential Cross Sections for 4.13 GeV/c π^- p; s = 8.65 $(GeV)^2$, $\ell n\ s = 2.16$

Cos θ	$\frac{d\sigma}{d\Omega}$ $\frac{mb}{sr}$	$-t\left[\frac{GeV}{c}\right]^2$ at Center of Interval	$-u\left[\frac{GeV}{c}\right]^2$ at Center of Interval	$\left[\frac{4\pi}{k\,\sigma_{tot}}\right]^2 \frac{d\sigma}{d\Omega}$
0.98 to 0.96	11.39 $\pm$0.58	0.104		0.4514 $\pm$0.0230
0.96 to 0.94	5.92 $\pm$0.34	0.173		0.2346 $\pm$0.0135
0.94 to 0.92	3.30 $\pm$0.24	0.243		0.1308 $\pm$0.0095
0.92 to 0.90	1.96 $\pm$0.19	0.312		0.0777 $\pm$0.0075
0.90 to 0.88	0.80 $\pm$0.12	0.382		0.0317 $\pm$0.0048
0.88 to 0.86	0.60 $\pm$0.10	0.451		0.0238 $\pm$0.0040
0.86 to 0.84	0.45 $\pm$0.09	0.520		0.0178 $\pm$0.0036
0.84 to 0.82	0.22 $\pm$0.06	0.590		0.0087 $\pm$0.0024
0.82 to 0.80	0.21 $\pm$0.06	0.659		0.0083 $\pm$0.0024
0.80 to 0.76	0.15 $\pm$0.05	0.763		0.0059 $\pm$0.0020
0.76 to 0.72	0.08 $\pm$0.04	0.902		0.0032 $\pm$0.0016
0.72 to 0.60	0.013$\pm$0.008	1.18		0.00052$\pm$0.00032
0.60 to 0.48	0.017$\pm$0.012	1.60	5.26	0.00067$\pm$0.00048
0.48 to -0.26	0.005$\pm$0.003	3.09	3.77	0.00020$\pm$0.00012
-0.26 to -0.48	$0.000^{+0.005}_{-0.000}$	4.75	2.10	$0.00000^{+0.00020}_{-0.00000}$
-0.48 to -0.93	$0.000^{+0.003}_{-0.000}$	5.92	0.940	$0.00000^{+0.00012}_{-0.00000}$

Table V

Elastic Scattering Differential Cross Sections for 4.95 GeV/c

$\pi^- p$; $s = 10.19\ (\mathrm{GeV})^2$, $\ell n\ s = 2.32$

Cos θ	$\frac{d\sigma}{d\Omega}\frac{mb}{sr}$	$-t\left[\frac{GeV}{c}\right]^2$ at Center of Interval	$-u\left[\frac{GeV}{c}\right]^2$ at Center of Interval	$\left[\frac{4\pi}{k\,\sigma_{tot}}\right]^2 \frac{d\sigma}{d\Omega}$
0.98 to 0.96	12.98 ± 0.65	0.127		0.4453 ± 0.0223
0.96 to 0.94	6.58 ± 0.30	0.212		0.2257 ± 0.0103
0.94 to 0.92	3.06 ± 0.22	0.296		0.1050 ± 0.0075
0.92 to 0.90	1.81 ± 0.18	0.381		0.0621 ± 0.0062
0.90 to 0.88	1.20 ± 0.14	0.466		0.0412 ± 0.0048
0.88 to 0.86	0.62 ± 0.10	0.550		0.0213 ± 0.0034
0.86 to 0.84	0.26 ± 0.07	0.635		0.0089 ± 0.0024
0.84 to 0.82	0.18 ± 0.06	0.720		0.0062 ± 0.0020
0.82 to 0.80	0.068 ± 0.030	0.804		0.0023 ± 0.0010
0.80 to 0.78	0.034 ± 0.025	0.889		0.0012 ± 0.00086
0.78 to 0.74	$0.000^{+0.014}_{-0.000}$	1.02		$0.0000^{+0.00048}_{-0.00000}$
0.74 to 0.57	$0.000^{+0.015}_{-0.000}$	1.46		$0.0000^{+0.00051}_{-0.00000}$
0. 7 to 0.38	$0.000^{+0.008}_{-0.000}$	2.22	6.17	$0.0000^{+0.00027}_{-0.00000}$
0.38 to -0.21	$0.000^{+0.002}_{-0.000}$	3.87	4.52	$0.0000^{+0.00007}_{-0.00000}$
-0.21 to -0.55	$0.000^{+0.008}_{-0.000}$	5.84	2.55	$0.0000^{+0.00027}_{-0.00000}$
-0.55 to -0.93	$0.000^{+0.006}_{-0.000}$	7.37	1.02	$0.0000^{+0.00020}_{-0.00000}$

Table VI

Values of the Coefficients in the Expression $d\sigma/d\Omega = \exp(A_0 + A_1 t)$ Fit to the Data Over Different Intervals of Four-Momentum Transfer, t

System		$\pi^+ p$	$\pi^- p$	$\pi^- p$	$\pi^- p$
p_{lab} (GeV/c)		2.92	3.15	4.13	4.95
minimum $\|t\|$ $(GeV/c)^2$		0.082	0.090	0.104	0.127
$0 < \|t\| < 0.4$ $(GeV/c)^2$	$\left(\frac{d\sigma}{d\Omega}\right)_0$ $\frac{mb}{sr}$	12.4 ±0.9	21.0 ±1.3	27.6 ±1.8	32.5 ±2.4
	A_0	2.52±0.07	3.04±0.06	3.32±0.07	3.48±0.07
	A_1 $(GeV/c)^2$	7.6 ±0.3	7.9 ±0.3	8.4 ±0.3	7.8 ±0.3
	P (χ^2)	0.20	0.02	0.20	0.10
$0.4 < \|t\| < 0.8$ $(GeV/c)^2$	A_1 $(GeV/c)^2$	5.6 ±0.7	5.2 ±1.0	4.7 ±0.6	7.8 ±0.8
	P (χ^2)	0.40	0.05	0.40	0.90
$0 < \|t\| < 0.8$ $(GeV/c)^2$	A_1 $(GeV/c)^2$	6.6 ±0.3	7.5 ±0.2	7.5 ±0.2	7.4 ±0.2
	P (χ^2)	$\ll$0.01	$\ll$0.01	$\ll$0.01	0.30

Table VII

Values of the Coefficients in the Expressions $d\sigma/d\Omega = \exp(A_0+A_1t+A_2t^2)$
Fit to the Data Over Different Intervals of Four-Momentum Transfer, t

System		π^+ p	π^- p	π^- p	π^- p
p_{lab} (GeV/c)		2.92	3.15	4.13	4.95
$0 < \|t\| < 0.4$ $(GeV/c)^2$	$\left(\frac{d\sigma}{d\Omega}\right)_0$ $\frac{mb}{sr}$	16.9 ±3.0	14.8 ±2.2	29.6 ±4.6	41.2 ±10.6
	A_0	2.8 ±0.2	2.7 ±0.2	3.4 ±0.2	3.7 ± 0.2
	A_1 $(GeV/c)^{-2}$	11.0 ±1.8	5.2 ±1.4	9.5 ±1.4	9.7 ± 2.3
	A_2 $(GeV/c)^{-4}$	7.2 ±3.8	- 7.4 ±2.8	1.4 ±2.7	3.6 ± 4.9
	P (χ^2)	0.60	0.15	0.05	0.40
$0 < \|t\| < 0.8$ $(GeV/c)^2$	$\left(\frac{d\sigma}{d\Omega}\right)_0$ $\frac{mb}{sr}$	14.2 ±1.4	22.0 ±2.2	35.7 ±3.5	34.3 ± 4.0
	A_0	2.7 ±0.3	3.1 ±0.1	3.6 ±0.1	3.5 ± 0.1
	A_1 (GeV/c)	9.2 +0.7	9.6 ±0.7	11.5 ±0.7	8.1 ± 0.7
	A_2 $(GeV/c)^{-4}$	4.0 ±1.1	2.9 ±1.1	5.5 ±0.9	0.9 ± 1.0
	P (χ^2)	0.20	$<<0.01$	0.20	0.30
$0 < \|t\| < 1.0$ $(GeV/c)^2$	$\left(\frac{d\sigma}{d\Omega}\right)_0$ $\frac{mb}{sr}$	13.5 ±1.3	22.6 ±1.9	33.6 ±2.8	32.6 ± 3.4
	A_0	2.60 ±0.09	3.12 ±0.08	3.51 ±0.08	3.48 ± 0.1
	A_1 $(GeV/c)^{-2}$	8.8 ±0.7	9.9 ±0.6	11.0 ±0.5	7.6 ± 0.7
	A_2 $(GeV/c)^{-4}$	3.2 ±1.0	3.2 ±0.8	4.7 ±0.7	0.3 ± 0.9
	P (χ^2)	0.10	$<<0.01$	0.10	0.40
$0 < \|t\| < 0.8$ $(GeV/c)^2$	$\left(\frac{d\sigma}{d\Omega}\right)_0$ $\frac{mb}{sr}$	12.5 ±1.0	20.9 ±1.6	30.9 ±2.3	32.8 ± 2.9
	A_0	2.53 ±0.08	3.04 ±0.08	3.43 ±0.08	3.49 ± 0.9
	A_1 $(GeV/c)^{-2}$	7.8 ±0.4	8.9 ±0.4	9.7 ±0.4	7.7 ± 0.4
	A_3 $(GeV/c)^{-6}$	- 3.1 ±1.0	- 3.0 ±1.2	- 4.7 ±0.7	- 0.5 ± 0.8
	P (χ^2)	0.05	0.01	0.30	0.30
$0 < \|t\| < 1.0$ $(GeV/c)^2$	$\left(\frac{d\sigma}{d\Omega}\right)_0$ $\frac{mb}{sr}$	11.9 ±0.9	20.4 ±1.3	28.1 ±1.8	31.6 ± 2.6
	A_0	2.48 ±0.07	3.02 ±0.06	3.34 ±0.07	3.45 ± 0.08
	A_1 $(GeV/c)^{-2}$	7.5 ±0.4	8.7 ±0.3	9.1 ±0.3	7.4 ± 0.4
	A_3 $(GeV/c)^{-6}$	- 2.1 ±0.8	- 2.5 ±0.6	- 3.2 ±0.5	0.04 ± 0.6
	P (χ^2)	0.05	$<<0.01$	0.10	0.40
$0 < \|t\| < \|t\|$ max $(GeV/c)^2$	$\|t\|$ max $(GeV/)^2$	4.1	4.35	5.9	7.4
	$\left(\frac{d\sigma}{d\Omega}\right)_0$ $\frac{mb}{sr}$	9.0 ±0.5	13.1 ±0.6	16.2 ±0.7	23.6 ± 1.2
	A_0	2.19 ±0.05	2.57 ±0.05	2.78 ±0.05	3.16 ± 0.05
	A_1 $(GeV/c)^{-2}$	6.1 ±0.2	6.4 ±0.5	6.3 ±0.4	6.3 ± 0.2
	A_3 $(GeV/c)^{-6}$	- 0.308±0.017	- 0.286±0.015	- 0.156±0.006	- 0.105± 0.005
	P (χ^2)	$<<0.01$	$<<0.01$	$<<0.01$	$<<0.01$

Table VIII

Total Cross Sections, σ_t, Values of $(k\sigma_t/4\pi)^2$, and Values of $(d\sigma/d\Omega)$ at 0° Extrapolated According to the Various Fits of Tables VI and VII

(The ratio, $\mathcal{R}$, of the extrapolated value of $(d\sigma/d\Omega)_0$ to $(k\sigma_t/4\pi)^2$ is tabulated in each instance. The total cross sections are taken from Refs. 26 and 27.)

System		$\pi^+ p$	$\pi^- p$	$\pi^- p$	$\pi^- p$
p_{lab} (GeV/c)		2.92	3.15	4.13	4.95
σ_{total} (mb)		28.7 ±0.5	31.3 ±0.5	29.9 ±0.5	29.1 ± 0.5
k (cm^{-1})		0.549×10^{14}	0.574×10^{14}	0.668×10^{14}	0.739×10^{14}
$\left(\frac{k\sigma_t}{4\pi}\right)^2 \frac{mb}{sr}$		15.8 ±0.5	20.4 ±0.7	25.2 ±0.8	29.2 ± 1.0
normalization uncertainty		±30%	±8%	±8%	±8%
exp (A_0+A_1t)	$\left(\frac{d\sigma}{d\Omega}\right)_0 \frac{mb}{sr}$	12.4 ±0.9	21.0 ±1.3	27.6±1.8	33.2 ± 2.7
$0 < \|t\| < 0.4$ (GeV/c)^2	$\mathcal{R}$	0.79±0.24	1.03±0.11	1.09±0.11	1.14± 0.14
exp $(A_0+A_1t+A_2t^2)$	$\left(\frac{d\sigma}{d\Omega}\right)_0 \frac{mb}{sr}$	16.9 ±3.0	14.8 ±2.2	29.6 ±4.5	41.2 ±10.1
$0 < \|t\| < 0.4$ (GeV/c)^2	$\mathcal{R}$	1.07±0.37	0.72±0.17	1.17±0.20	1.41± 0.35
exp $(A_0+A_1t+A_2t^2)$	$\left(\frac{d\sigma}{d\Omega}\right)_0 \frac{mb}{sr}$	14.2 ±1.5	22.0 ±2.2	35.7 ±3.4	34.3 ± 3.9
$0 < \|t\| < 0.8$ (GeV/c)^2	$\mathcal{R}$	0.90±0.29	1.08±0.14	1.41±0.18	1.18± 0.14

Table IX

Total Cross Sections, σ_t, and Total Elastic Cross Sections, $\sigma_{elastic}$, Where $\sigma_{elastic}$ is the Integral Under the Data Points Plus the Contribution from $t = 0$ to the First Data Point Taken According to the Fits of Tables VI and VII

(In the case of the $\pi^+ p$ data, where normalization is less certain, a value of $\sigma_{elastic}$ is also given in which the data are scaled so that the linear fit passes through the optical theorem point $(k\sigma_t/4\pi)^2$.)

System	$\pi^+ p$	$\pi^- p$	$\pi^- p$	$\pi^- p$
p_{lab} (GeV/c)	2.92	3.15	4.13	4.95
σ_{total} (mb)	28.7±0.5	31.3±0.3	29.9±0.5	29.1±0.5
$\sigma_{elastic}$ (mb) for:				
1. exp (A_0+A_1t) fit:				
$0 < \|t\| < 0.4$ (GeV/c)^2	4.6±1.5	6.2±0.7	5.9±0.6	6.5±0.7
$\sigma_{elastic}/\sigma_{total}$	16%	19.8%	19.7%	22.7%
2. exp $(A_0+A_1t+A_2t^2)$ fit:				
$0 < \|t\| < 0.8$ (GeV/c)^2	4.8±1.0	6.4±0.8	6.3±0.8	6.5±0.8
$\sigma_{elastic}/\sigma_{total}$	16.7%	20.4%	21.0%	22.4%
3. fit to optical point exp (A_0+A_1t)				
$0 < \|t\| < 0.8$ (GeV/c)^2	5.1±1.0	6.1±0.7	5.6±0.6	6.1±0.7
$\sigma_{elastic}/\sigma_{total}$	17.8%	19.5%	18.7%	21.0%
4. Normalization shifted to allow linear fit to pass through optical point	5.9±1.0			
$\sigma_{elastic}/\sigma_{total}$	20.6%			

Table X

Nuclear Radius R and Opacity (1-a) Calculated from a Simple Optical Model to Fit to the Data at Each Energy

System	π^+ p	π^- p	π^- p	π^- p
p_{lab} (GeV/c)	2.92	3.15	4.13	4.95
kR	6.25±0.3	6.25±0.3	7.05±0.3	7.25±0.3
R (10^{-13} cm)	1.14±0.05	1.09±0.05	1.05±0.05	0.98±0.04
(1-a)	0.35±0.04	0.42±0.04	0.43±0.04	0.47±0.04
P (χ^2)	0.04	<0.01	0.10	0.05

Table XI

Values of the Coefficients in the Expression

$$d\sigma/d\Omega = \exp (A_0+A_1t+A_2t^2+A_3t^3+A_4t^4)$$

Fit to the Data Over the Ranges of Four-Momentum Transfer t Indicated

System	π^+ p	π^- p	π^- p	π^- p
p_{lab} (GeV/c)	2.92	3.15	4.13	4.95
A_0	2.65±0.09	3.25±0.08	3.50±0.08	3.64±0.08
A_1 $(GeV/c)^{-2}$	9.3 ±0.7	11.2 ±0.6	11.0 ±0.5	8.9 ±0.5
A_2 $(GeV/c)^{-4}$	4.4 ±1.2	6.2 ±1.1	5.5 ±0.7	2.0 ±0.6
A_3 $(GeV/c)^{-6}$	0.7 ±0.6	1.5 ±0.5	1.2 ±0.2	0.1 ±0.6
A_4 $(GeV/c)^{-8}$	0.02±0.08	0.13±0.08	0.09±0.02	0.00±0.01
P (χ^2)	0.20	$\ll$0.01	0.15	0.05
Maximum $\lvert t \rvert$ $(GeV/c)^2$	4.1	4.4	5.9	7.4

Table XII

Data for π^- p Elastic Scattering in the Backward (c.m.) Hemisphere, and in the Steradian Centered at $\theta = 1.80°$ from Various Experiments Including the Present One

(All cross sections are in μb/sr.)

System	Incident Pion Laboratory Momentum (GeV/c)	μb/sr $-1.0 < \cos\theta < 0$	μb/sr for the Last Steradian in c.m. System $-1.0 < \cos\theta < -0.841$	θ_{max} (c.m.)	Reference
π^- p	1.43-1.51	300 ± 60	300 ± 150	180°	a,b
π^- p	2.0	150^{+30}_{-50}		152°	b
π^- p	2.5	100^{+20}_{-50}		149°	b
π^- p	2.8		< 30	180°	c
π^- p	2.8	100 ± 40		180°	d
π^- p	3.15	4^{+10}_{-3}	8^{+10}_{-8}	157°	This exp.
π^- p	4.13	< 5	< 5	158°	This exp.
π^- p	4.95	< 6	< 10	158°	This exp.
π^- p	7.0-8.0		< 30	180°	e
π^+ p	1.5	760 ± 150	650^{+600}_{-300}	158°	f
π^+ p	1.69	320 ± 30	250 ± 150	164°	g
π^+ p	2.0	200 ± 40	40 ± 40	158°	f
π^+ p	2.5	70 ± 30	80 ± 60	162°	f
π^+ p	2.8		< 14	180°	h
π^+ p	2.8	6 ± 6		180°	i
π^+ p	2.92	18 ± 11	13 ± 11	157°	This exp.
π^+ p	7.0-8.0		< 90	180°	e
π^+ p	3.14		at 180° $d\sigma/d\Omega = 920 \pm 470$ μb/sr		j
π^+ p	4.6		at 180° $d\sigma/d\Omega = 380 \pm 240$ μb/sr		j

a. M. Chretien et al., Phys. Rev. 108, 383 (1957).

b. K. W. Lai et al., Phys. Rev. Letters 7, 125 (1961).

c. Yu. D. Bayukov et al., Soviet Physics—JETP 14, 1432 (1962).

d. L. P. Kotenko et al., Soviet Physics—JETP 15, 800 (1962).

e. R. A. Aripov et al., Soviet Physics—JETP 14, 946 (1962).

f. V. Cook et al., Phys. Rev. 130, 762 (1963).

g. J. A. Helland, UCRL Report 10378 (1962).

h. Yu. D. Bayukov et al., Soviet Physcis—JETP 14, 40 (1962). (This is a $\pi^- + n \to \pi^- + n$ measurement and charge independence is assumed.)

i. Yu. D. Bayukov et al., Soviet Physics—JETP 14, 729 (1962).

j. B. A. Kulakov et al., Proceedings of the 1962 International Conference on High-Energy Physics at CERN (CERN, Geneva, 1962), p. 584.

Table XIII

Values of the Coefficients in the Expression $d\sigma/d\Omega = \exp(A_0+A_1 t)$ in the Range of Four-Momentum Transfer $0 < |t| < 0.4$ $(GeV/c)^2$ and the Expression $d\sigma/d\Omega = \exp(A_0+A_1 t+A_2 t^2)$ in the Range of Four-Momentum Transfer $0 < |t| < 0.8$ $(GeV/c)^2$ for Proton-Proton Elastic Scattering

Proton Kinetic Energy GeV		6.15	4.40	2.87	2.85	2.24	2.10	2.00	1.35
s $(GeV)^2$		15.1	11.8	8.9	8.9	7.7	7.5	7.3	6.1
ℓn s		2.71	2.47	2.19	2.19	2.04	2.00	1.99	1.81
$0 < \|t\| < (0.4)$	A_0	4.0±0.15	3.9±0.1	3.7±0.06	3.8±0.06	3.4±0.09	3.5±0.05	3.5±0.05	3.1±0.04
	A_1	7.4±0.7	7.5±0.5	7.7±0.3	7.0±0.3	5.5±0.3	6.9±0.3	6.3±0.2	5.9±0.2
	P (χ^2)	0.10	0.50	0.01	0.99	0.99	0.80	0.40	0.90
$0 < \|t\| < 0.8$	A_0	4.2±0.8	4.0±0.14	3.9±0.06	3.8±0.07	3.8±0.15	3.6±0.06	3.6±0.06	
	A_1	9.4±2.0	8.8±0.8	8.9±0.8	6.9±0.5	8.2±0.7	8.2±0.5	6.7±0.5	
	A_2	3.4±3.2	3.8±0.8	3.7±0.3	0.6±0.6	3.6±0.7	3.6±0.7	1.1±0.7	
	P (χ^2)	0.15	0.15	0.15	0.05	0.30	0.20	0.20	
Reference		a	a	b	c	a	b	d	b

a. B. Cork, W. A. Wenzel, and C. W. Causey, Jr., Phys. Rev. 107, 859 (1957).

b. T. Fujii et al., Phys. Rev. 128, 1836 (1962).

c. G. A. Smith et al., Phys. Rev. 123, 2160 (1961); G. A. Smith, Thesis (Yale, 1962) (unpublished).

d. W. F. Fickinger et al., Phys. Rev. 125, 2082 (1962); W. F. Fickinger, private communication.

TABLE XIV

Values of the Coefficient A_1 in the Expression $d\sigma/d\Omega = \exp(A_0+A_1 t)$ Over the Range of Four-Momentum Transfer $0 < |t| < 0.4$ $(GeV/c)^2$ for Lower Energy π^- p Elastic Scattering Experiments

System	π^- p	π^- p	π^- p
p_{lab} (GeV/c)	1.34	1.43-1.51	2.0
A_1	7.3±0.4	7.3±0.6	8.7±0.5
P (χ^2)	0.25	0.45	0.20
s $(GeV)^2$	3.41	3.64	4.65
ℓn s	1.23	1.29	1.54
Reference	a	b,c	b,d

a. L. Bertanza et al., Nuova Cimento 19, 467 (1961).

b. K. W. Lai, L. W. Jones, and M. L. Perl, Phys. Rev. Letters 1, 125 (1961).

c. M. Chretien et al., Phys. Rev. 108, 383 (1957).

d. V. Cook et al., Phys. Rev. 123, 320 (1961).

Table XV

Average Values of A_1 and A_2 for Fits to All the Data Tabulated Above for the Expression $d\sigma/d\Omega = \exp(A_0+A_1t+A_2t^2)$ Over the Range of Four-Momentum Transfer $0 < |t| < 0.8$ $(GeV/c)^2$

System	p p	π^- p
A_1 $(GeV/c)^{-2}$	7.9 ± 0.2	9.6 ± 0.4
A_2 $(GeV/c)^{-4}$	2.7 ± 0.3	3.3 ± 0.5

FIGURE CAPTIONS

Fig. 1. The functions $[J_1(kR\theta)/kR\theta]^2$ and $[B(kR\theta)]^2$ vs. $kR\theta$.

Fig. 2. Feynman diagrams for backward elastic pion-nucleon scattering for the cases (a) $\pi^+ p \to \pi^+ p$ with neutron exchange, (b) $\pi^- p \to \pi^- p$ with doubly-charged 3/2-3/2 nucleon isobar exchange, and (c) $\pi p \to \pi p$ with one nucleon and two or more pions exchanged.

Fig. 3. Schematic, scale diagram of the experimental arrangement. SC1-SC6 are spark chambers, the black bars labelled C are coincidence scintillation counters, and those labelled A are anticoincidence counters. The axial cylinder indicates the location of the 18-in. liquid hydrogen target.

Fig. 4. Photograph of an elastic scattering event taken from the data film. Here 18 views of the 9 separate spark chambers combined on one film may be seen. The liquid hydrogen target lies behind the fiducial plane containing the roman numerals.

Fig. 5. Kinematics of laboratory scattering angles for 4.0 GeV/c elastic πp scattering, with a typical data point shown to illustrate the meaning of the distance D. The two possible curves for a given measured pair of angles are shown where, for curve I, $\theta_A = \theta_\pi$, $\theta_B = \theta_P$; and for curve II, $\theta_A = \theta_P$ and $\theta_B = \theta_\pi$.

Fig. 6. Elastic scattering differential cross sections for 2.92 GeV/c π^+ p. The errors shown are statistical. An additional normalization uncertainty of $^{+30}_{-10}$%, is not indicated. The open circle at t = 0 is the optical theorem prediction.

Fig. 7. Elastic scattering differential cross sections for 3.15 GeV/c π^- p. The errors shown are statistical. An additional normalization uncertainty of ±8% is not indicated. The open circle at t = 0 is the optical theorem prediction.

Fig. 8. Elastic scattering differential cross sections for 4.13 GeV/c π^- p. The errors shown are statistical. An additional normalization uncertainty of ±8% is not indicated. The open circle at t = 0 is the optical theorem prediction.

Fig. 9. Elastic scattering differential cross sections for 4.95 GeV/c π^- p. The errors shown are statistical. An additional normalization uncertainty of ±8% is not indicated. The open circle at t = 0 is the optical theorem prediction.

Fig. 10. Normalized elastic differential cross sections for the π^- p data superposed on one graph. Error bars are not shown in order to clarify close-lying points.

Fig. 11. Normalized elastic differential cross sections for all data from this experiment plotted on a log-log scale in order to examine possible power law dependence. Error bars are not shown.

Fig. 12. Elastic scattering differential cross sections for 2.92 GeV/c π^+ p over a limited t range together with the fitted curve $d\sigma/d\Omega = \exp(A_0+A_1t+A_2t^2)$ over the range $0 < |t| < 0.8$ $(GeV/c)^2$. The open circle at t = 0 is the optical model prediction.

Fig. 13. Elastic scattering differential cross sections for 3.15 GeV/c π^- p over a limited t range together with the fitted curve $d\sigma/d\Omega = \exp(A_0+A_1t+A_2t^2)$ over the range $0 < |t| < 0.8$ $(GeV/c)^2$. The open circle at t = 0 is the optical model prediction.

Fig. 14. Elastic scattering differential cross sections for 4.13 GeV/c π^- p over a limited t range together with the fitted curve $d\sigma/d\Omega = \exp(A_0+A_1t+A_2t^2)$ over the range $0 < |t| < 0.8$ $(GeV/c)^2$. The open circle at t = 0 is the optical model prediction.

Fig. 15. Elastic scattering differential cross sections for 4.95 GeV/c π^- p over a limited t range together with the fitted curve $d\sigma/d\Omega = \exp(A_0+A_1t+A_2t^2)$ over the range $0 < |t| < 0.8$ $(GeV/c)^2$. The open circle at t = 0 is the optical model prediction.

FIGURE CAPTIONS (Concluded)

Fig. 16. Normalized differential elastic scattering cross sections for the three π^- p data sets plotted vs. ℓns, with straight lines fitted through points of the same four-momentum transfer. The points are interpolated from the data of Tables III, IV, and V, with error bars indicated which include statistical errors of the data as well as interpolation and normalization uncertainties.

Fig. 17. The coefficient $A_1(\text{GeV/c})^{-2}$ vs. ℓns from linear fits to p p and π p elastic scattering data according to $d\sigma/d\Omega = \exp(A_0+A_1 t)$ in the range $0 < |t| < 0.4\ (\text{GeV/c})^2$. The straight lines are fitted to the plotted points for p p and π p scattering considered separately.

Fig. 18. Data for π p normalized elastic scattering differential cross section for $|t| > 0.4\ (\text{GeV/c})^2$ with smooths curves from p p elastic scattering differential cross section at $s = 7.5$ and $11.8\ (\text{GeV})^2$ plotted for comparison.

FOOTNOTES

*Supported by the U.S. Office of Naval Research.

**Present address Stanford University, Palo Alto, California

†A.E.C. Predoctoral Fellow. Currently at CERN, Geneva, Switzerland.

Footnotes to Fig. 15.

a. B. Cork, W. A. Wenzel, and C. W. Causey, Jr., Phys. Rev. 107, 859 (1957).

b. T. Fujii et al., Phys. Rev. 128, 1836 (1962).

c. G. A. Smith et al., Phys. Rev. 123, 2160 (1961).

G. A. Smith, Thesis (Yale, 1962) unpublished.

d. W. F. Finkinger et al., Phys. Rev. 125, 2082 (1962).

W. F. Finkinger, private communication.

e. L. Bertanza et al., Nuovo Cimento 19, 467 (1961).

f. K. W. Lai, L. W. Jones and M. L. Perl, Phys. Rev. Letters 7, 125 (1961).

g. M. Chretien et al., Phys. Rev. 108, 383 (1957).

h. V. Cook et al., Phys. Rev. 123, 320 (1961).

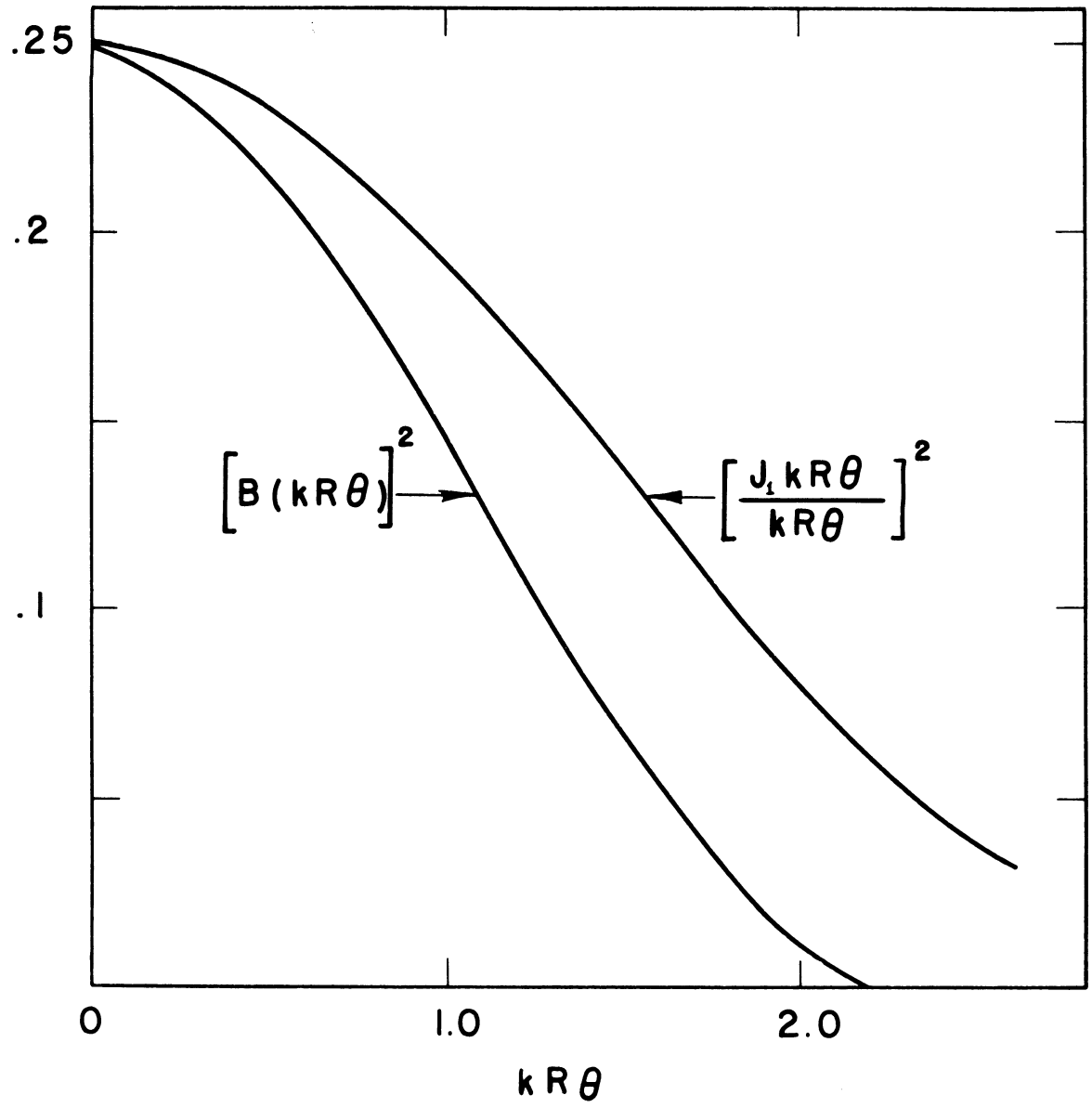

Fig. 1

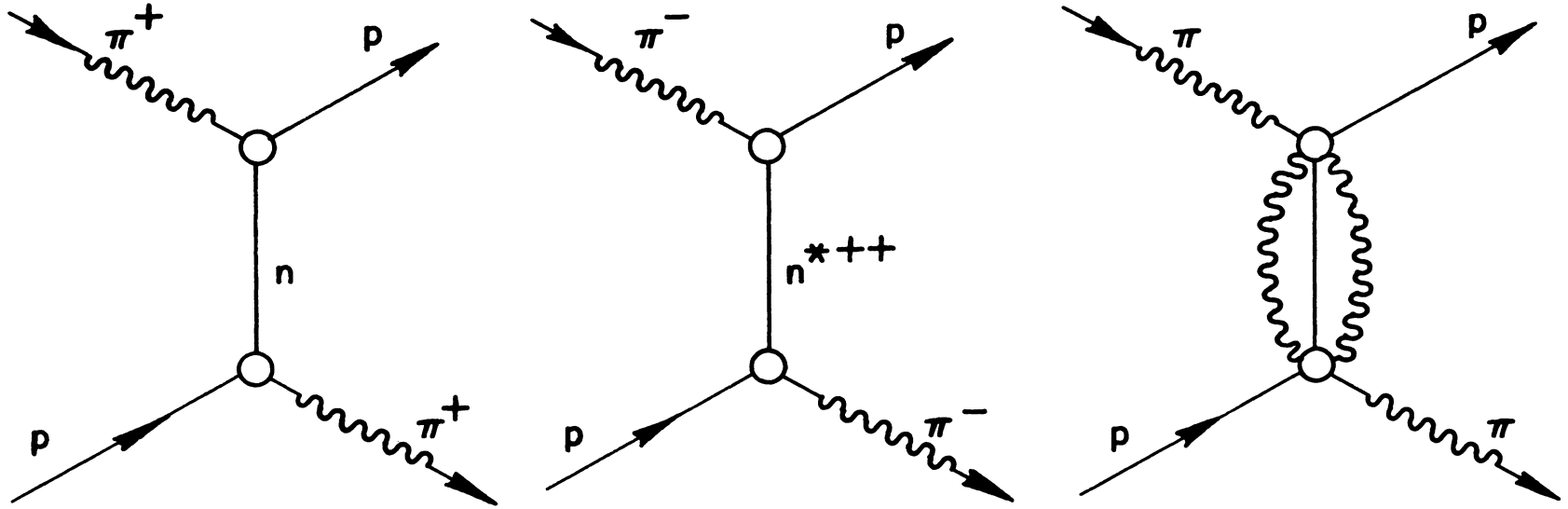

Fig. 2

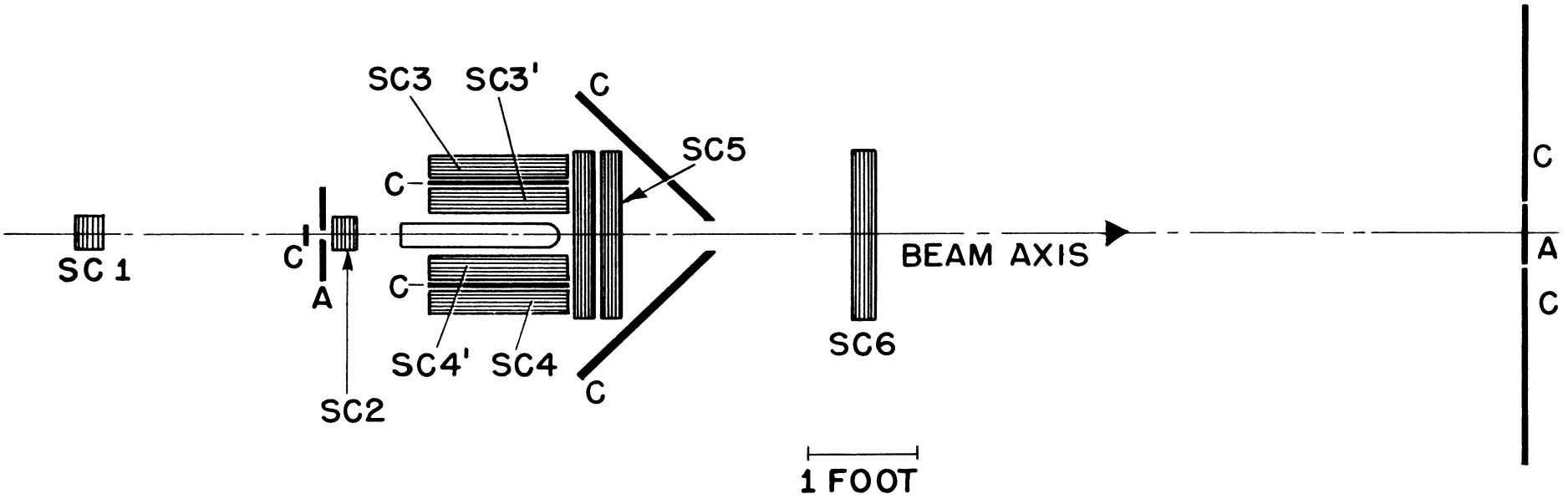

Fig. 3

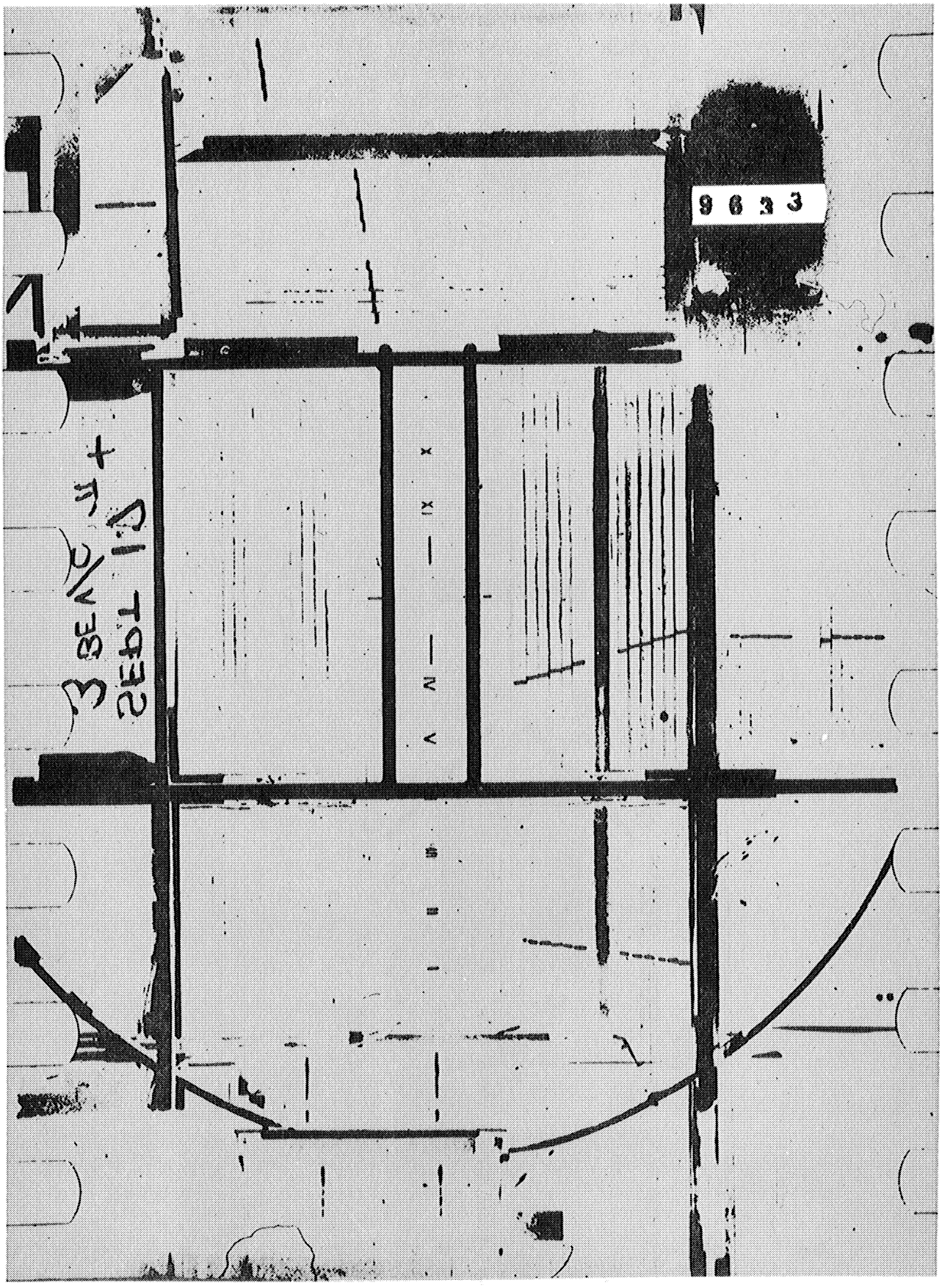

Fig. 4

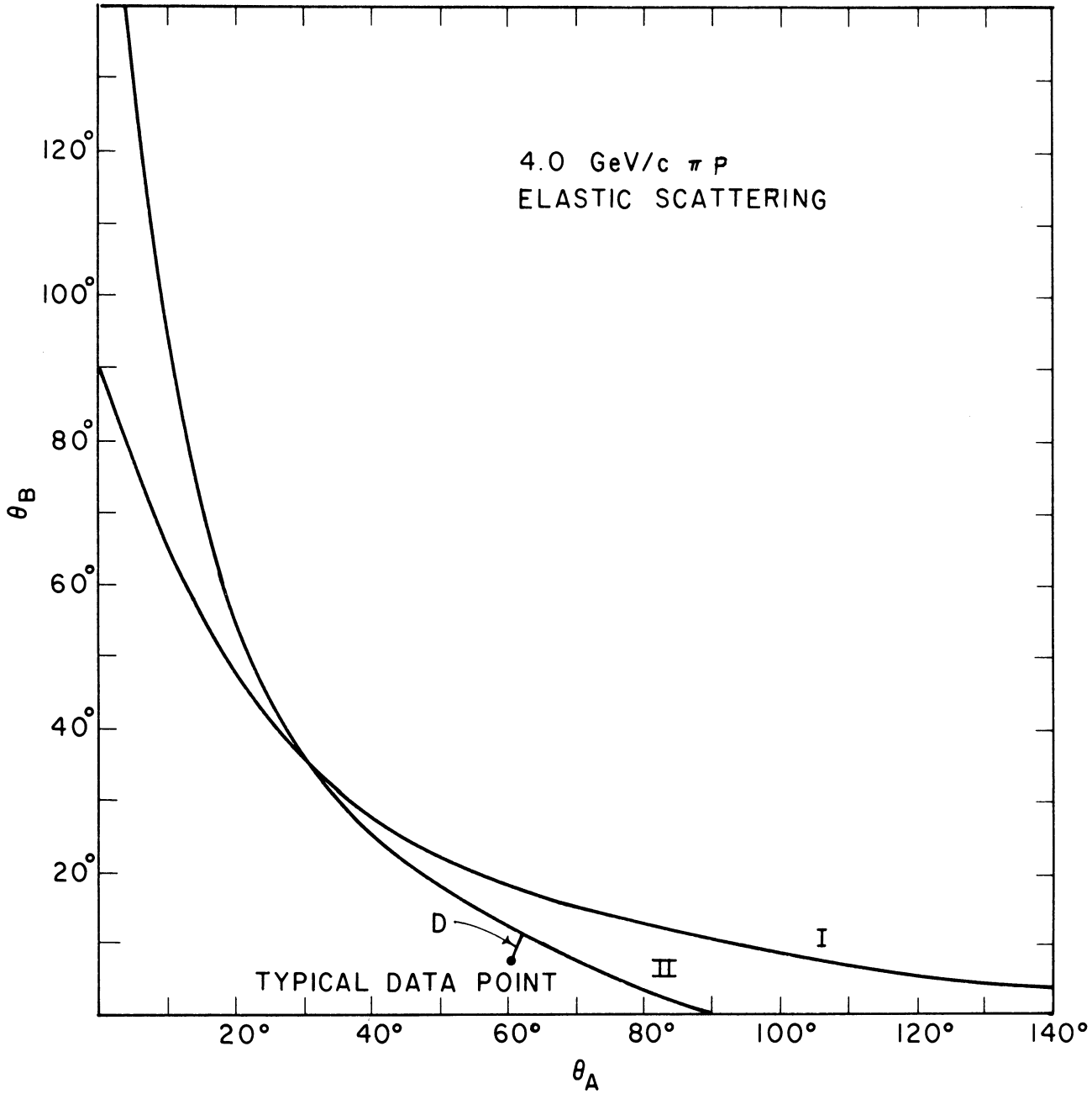
4.0 GeV/c π P
ELASTIC SCATTERING
120°
100°
80°
60°
40°
20°
θB
D
TYPICAL DATA POINT
I
II
20°
40°
60°
80°
100°
120°
140°
θA

Fig. 5

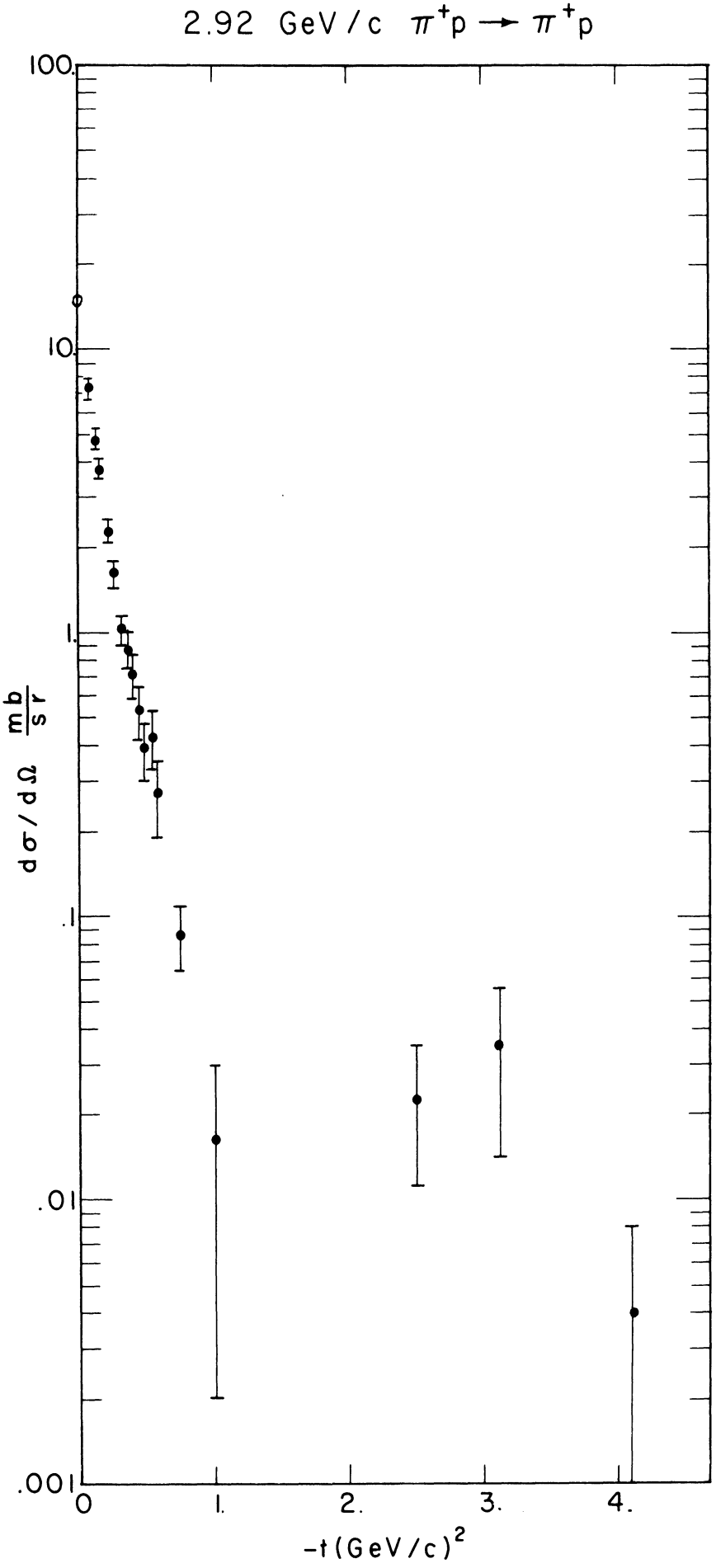
2.92 GeV/c $\pi^+ p \rightarrow \pi^+ p$
100.
10.
1.
.1
.01
.001
0
1.
2.
3.
4.
$d\sigma/d\Omega$ $\frac{mb}{sr}$
$-t(GeV/c)^2$

Fig. 6

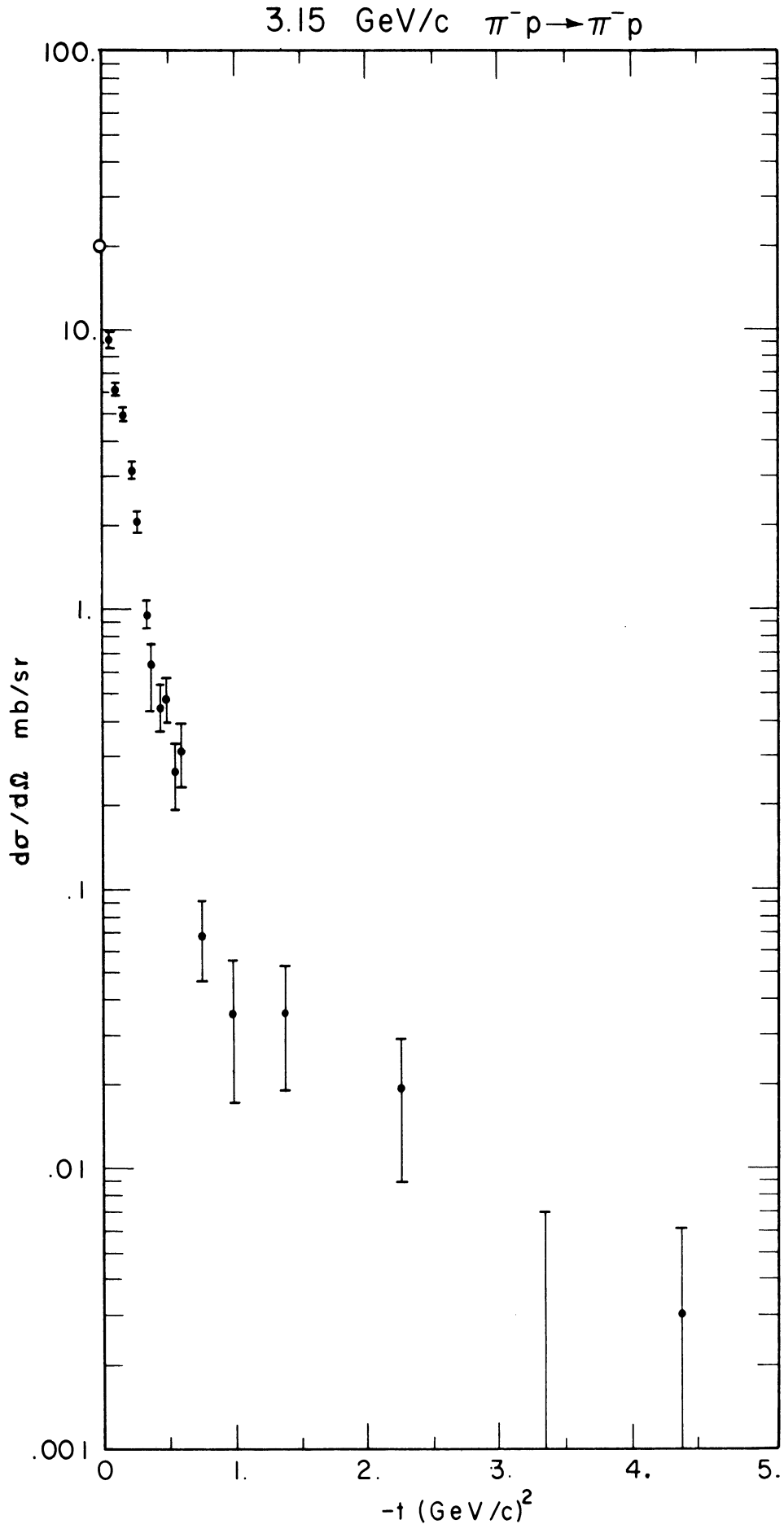
3.15 GeV/c $\pi^- p \rightarrow \pi^- p$
100.
10.
1.
.1
.01
.001
$d\sigma/d\Omega$ mb/sr
0
1.
2.
3.
4.
5.
$-t$ (GeV/c)^2

Fig. 7

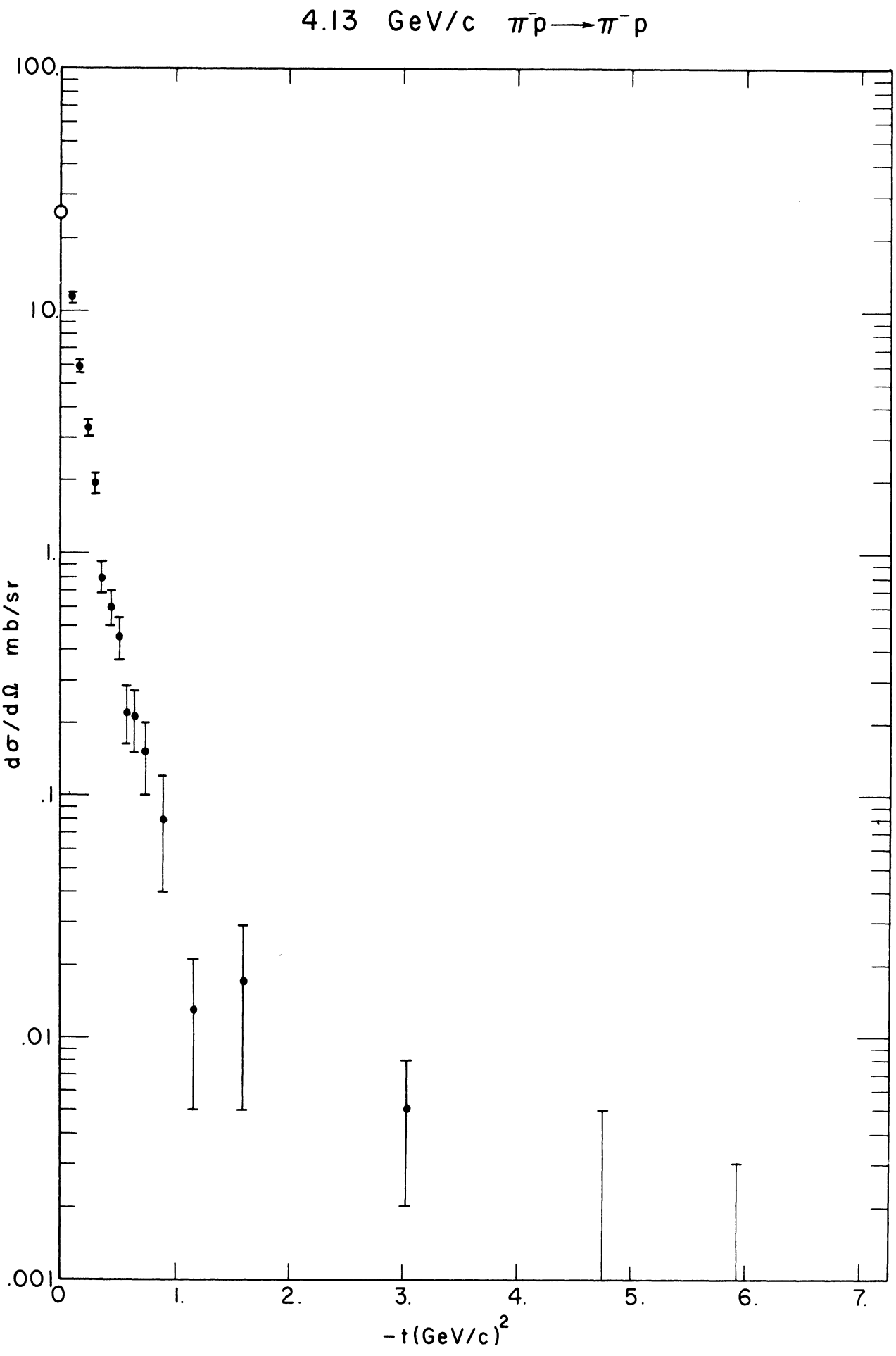
4.13 GeV/c $\pi^- p \longrightarrow \pi^- p$
100.
10.
1.
.1
.01
.001
$d\sigma/d\Omega$ mb/sr
0
1.
2.
3.
4.
5.
6.
7.
$-t(GeV/c)^2$

Fig. 8

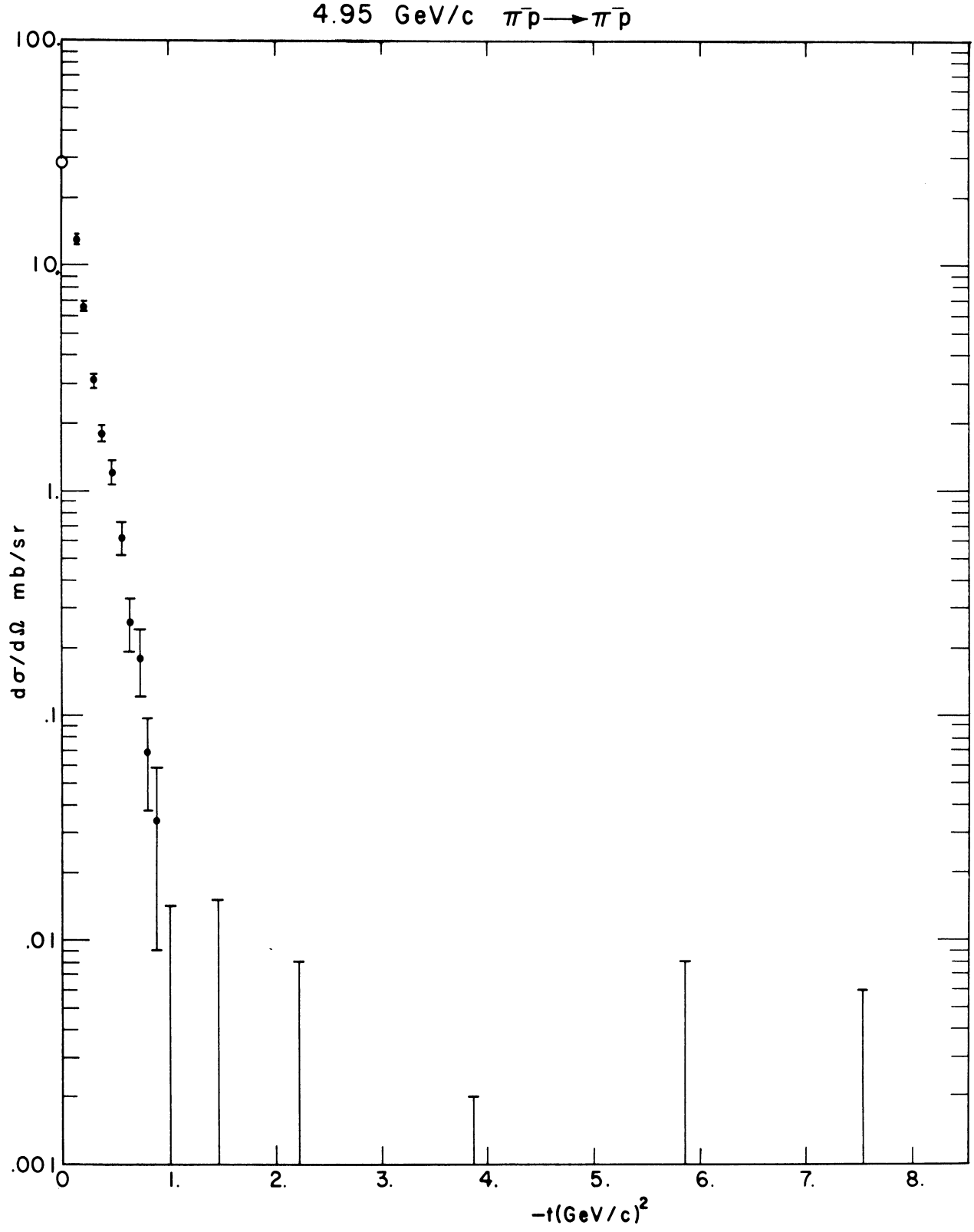
4.95 GeV/c $\pi^- p \rightarrow \pi^- p$
100.
10.
1.
.1
.01
.001
$d\sigma/d\Omega$ mb/sr
0
1.
2.
3.
4.
5.
6.
7.
8.
$-t(GeV/c)^2$

Fig. 9

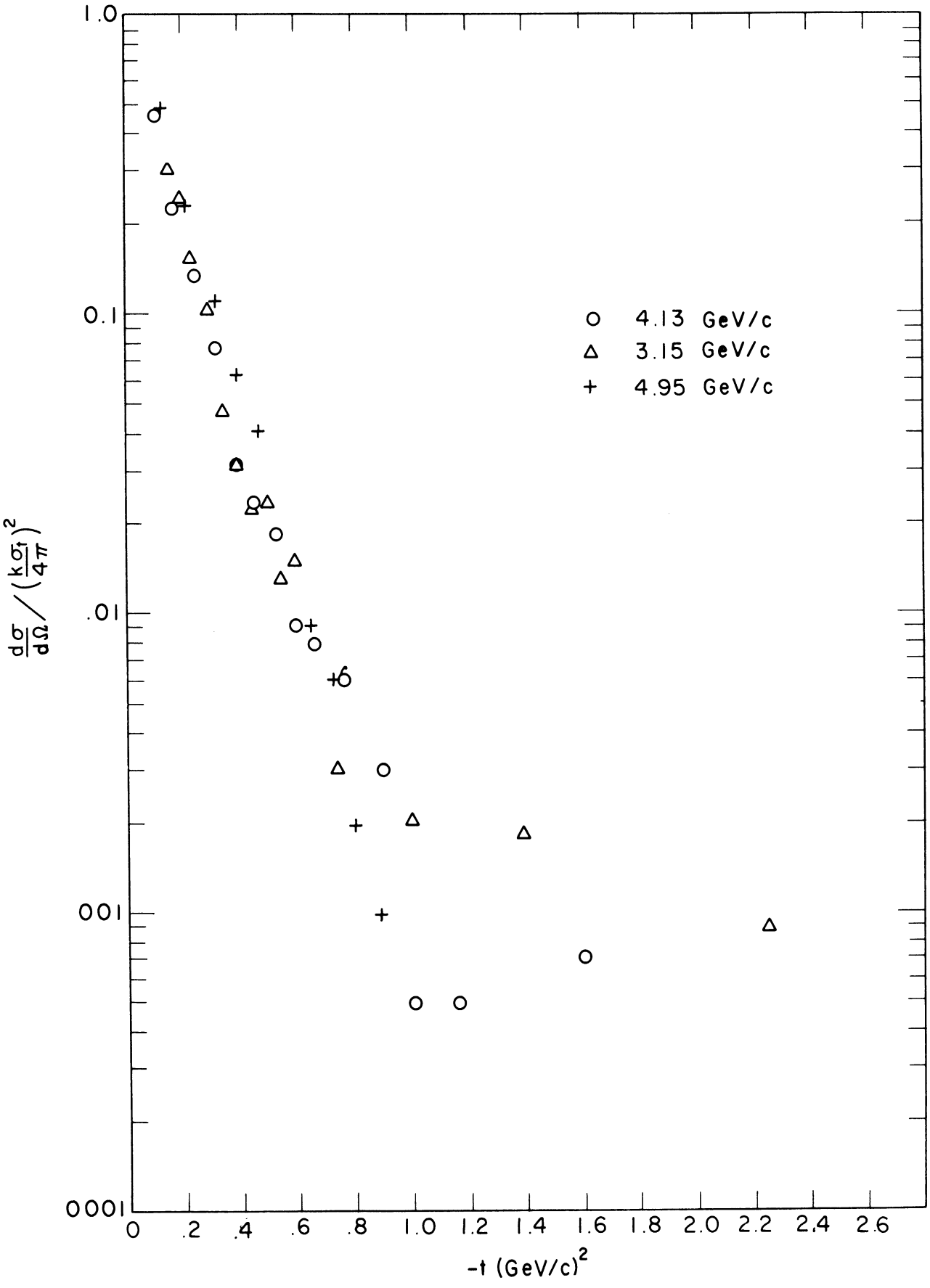
1.0
0.1
.01
001
0001
0
.2
.4
.6
.8
1.0
1.2
1.4
1.6
1.8
2.0
2.2
2.4
2.6
$\frac{d\sigma}{d\Omega} / \left(\frac{k\sigma_t}{4\pi}\right)^2$
$-t\ (GeV/c)^2$
4.13 GeV/c
3.15 GeV/c
4.95 GeV/c

Fig. 10

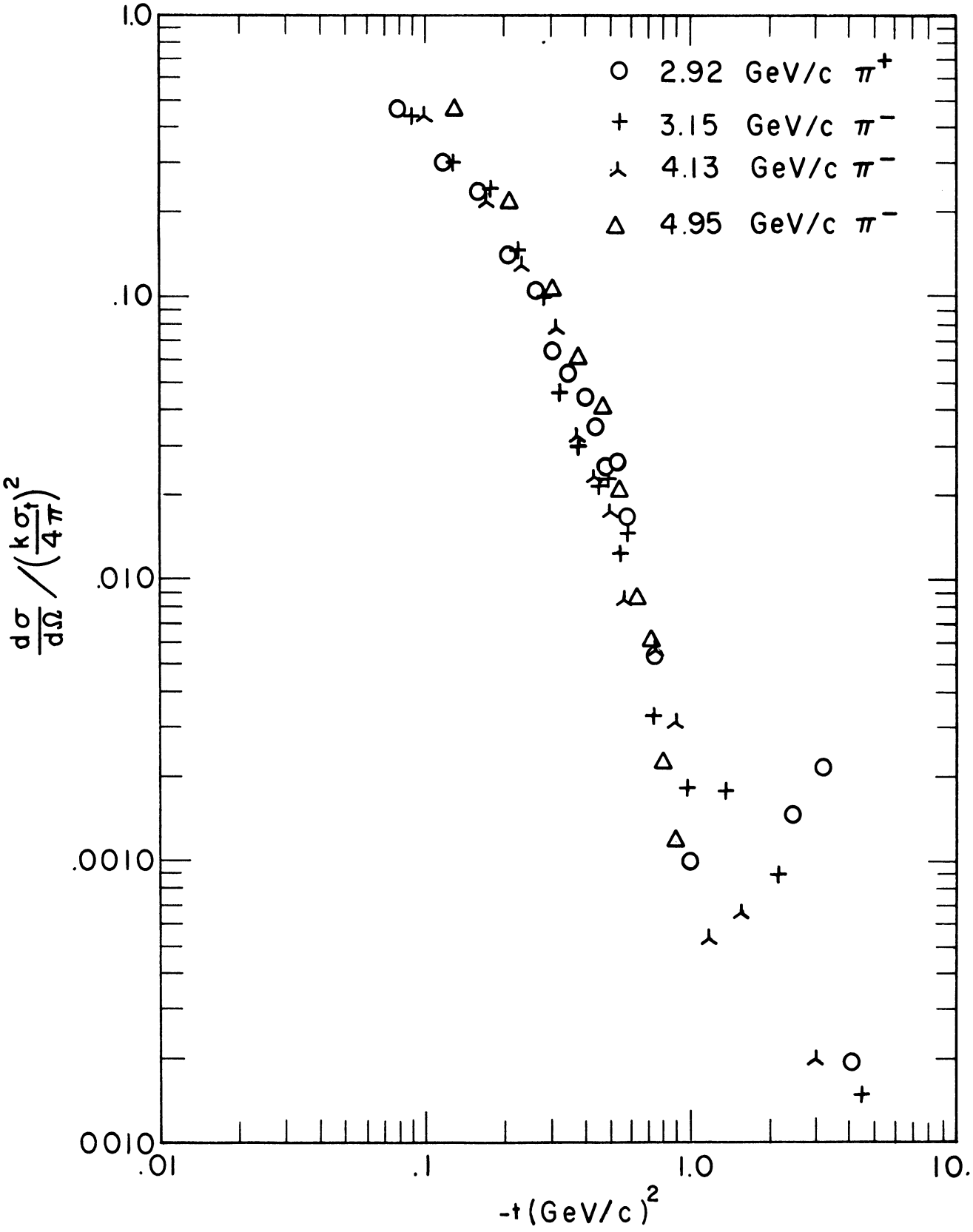
1.0
.10
.010
.0010
0010
.01
.1
1.0
10.
2.92 GeV/c π+
3.15 GeV/c π−
4.13 GeV/c π−
4.95 GeV/c π−
dσ/dΩ / (kσt/4π)²
-t (GeV/c)²

Fig. 11

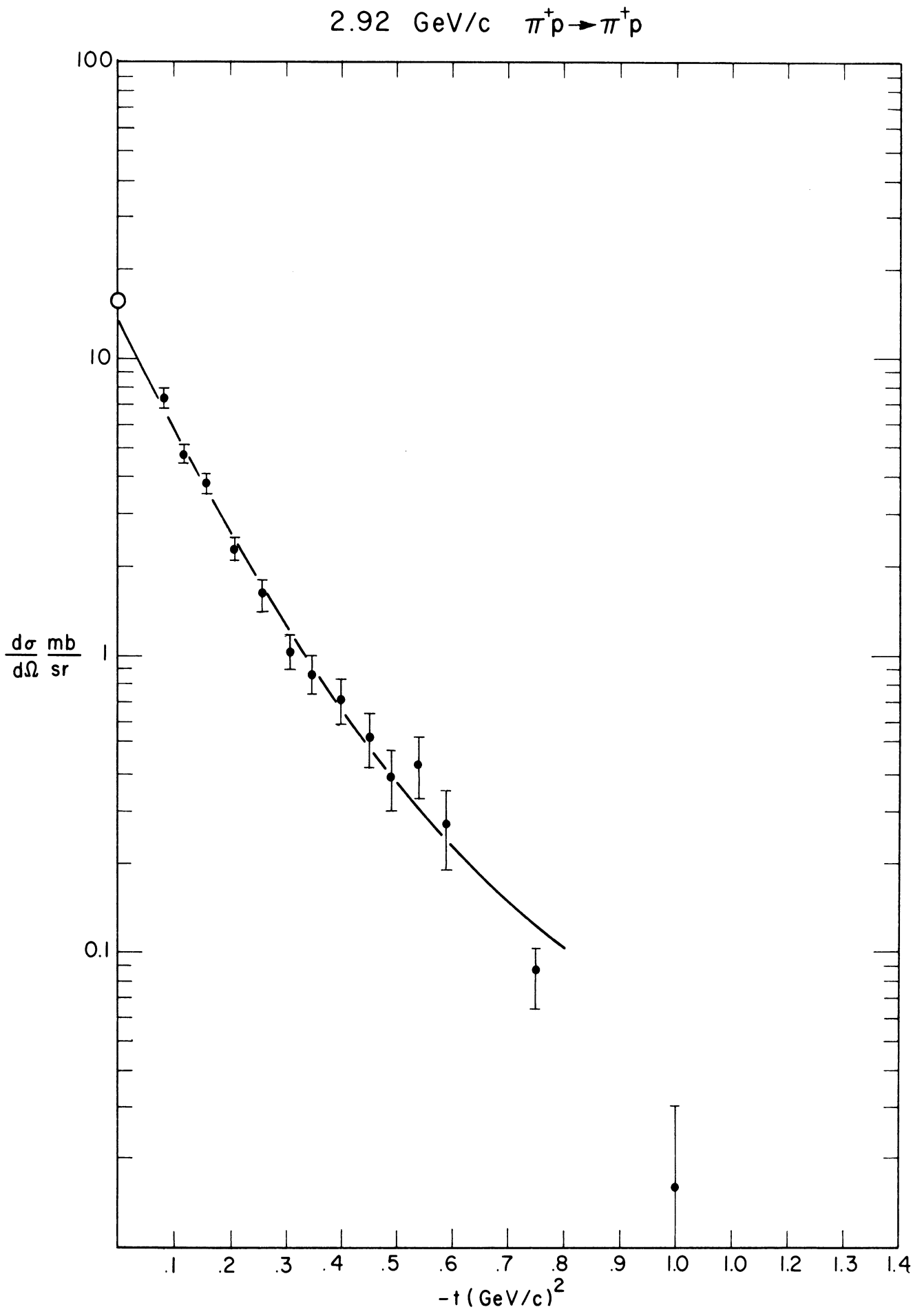
2.92 GeV/c $\pi^+p \rightarrow \pi^+p$
100
10
1
0.1
$\frac{d\sigma}{d\Omega}\frac{mb}{sr}$
.1
.2
.3
.4
.5
.6
.7
.8
.9
1.0
1.0
1.2
1.3
1.4
$-t\,(GeV/c)^2$

Fig. 12

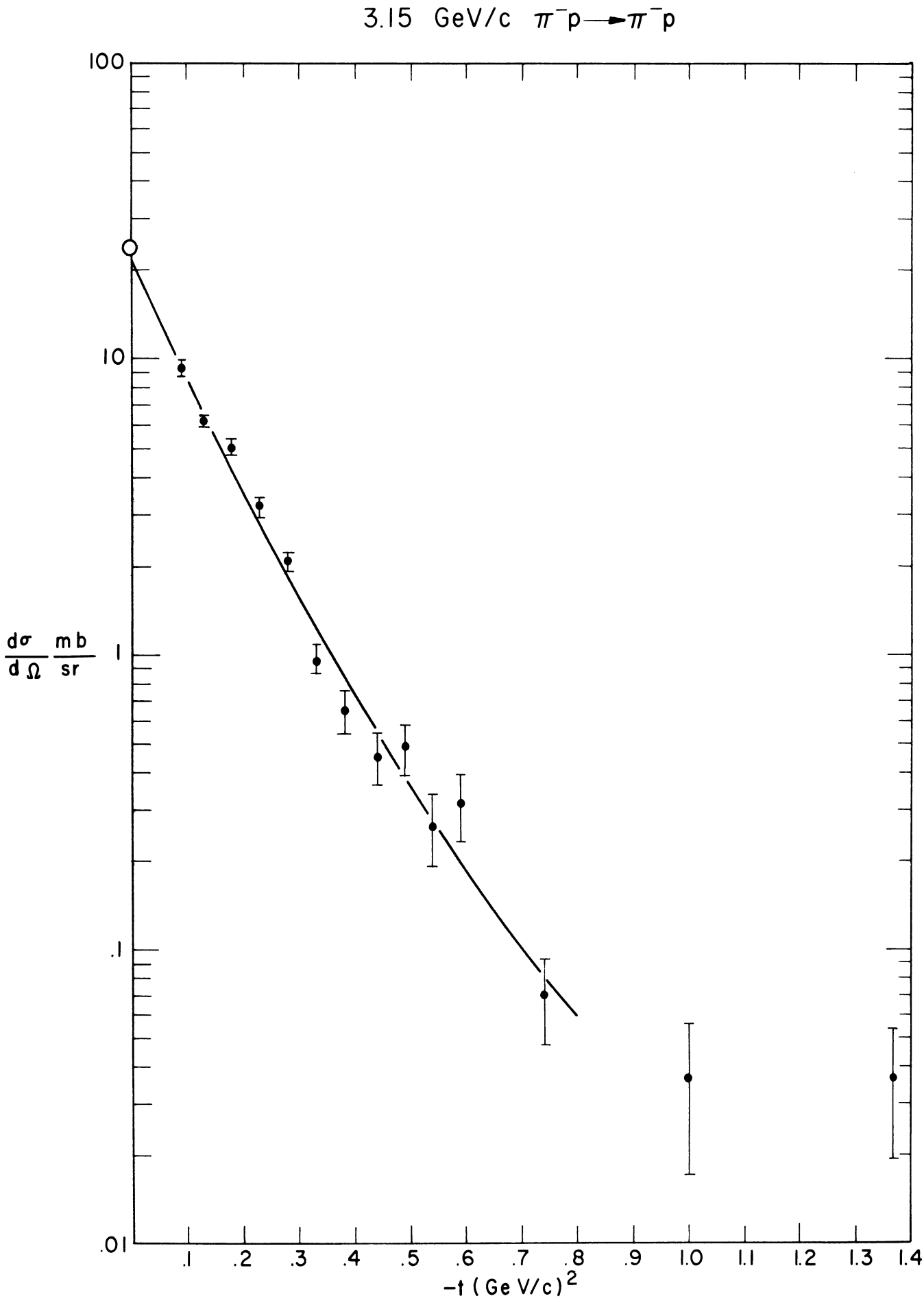
3.15 GeV/c $\pi^- p \rightarrow \pi^- p$
100
10
1
.1
.01
$\frac{d\sigma}{d\Omega}\frac{mb}{sr}$
.1
.2
.3
.4
.5
.6
.7
.8
.9
1.0
1.1
1.2
1.3
1.4
$-t\ (GeV/c)^2$

Fig. 13

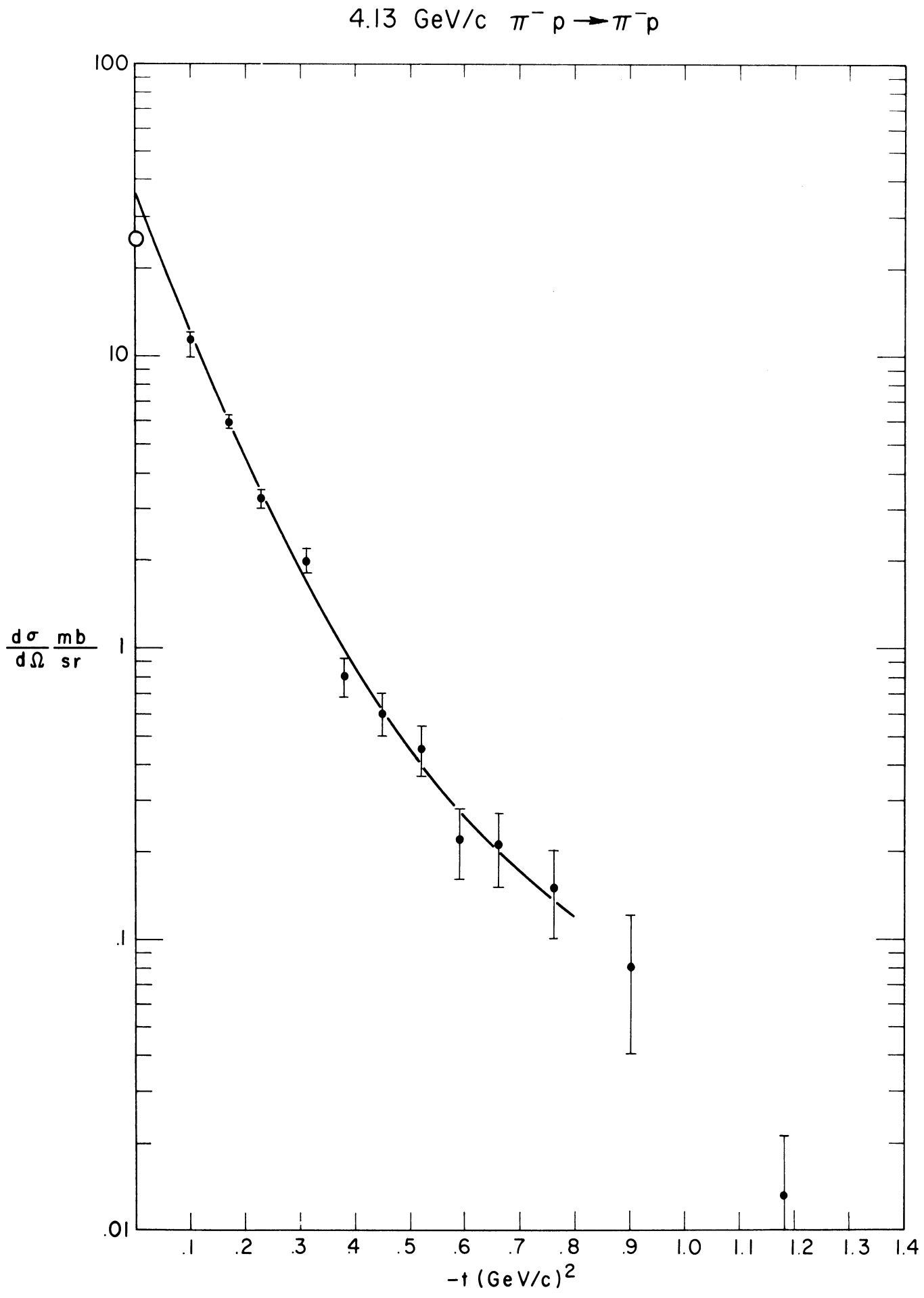
4.13 GeV/c $\pi^- p \rightarrow \pi^- p$
100
10
1
.1
.01
$\frac{d\sigma}{d\Omega} \frac{mb}{sr}$
.1
.2
.3
.4
.5
.6
.7
.8
.9
1.0
1.1
1.2
1.3
1.4
$-t\ (GeV/c)^2$

Fig. 14

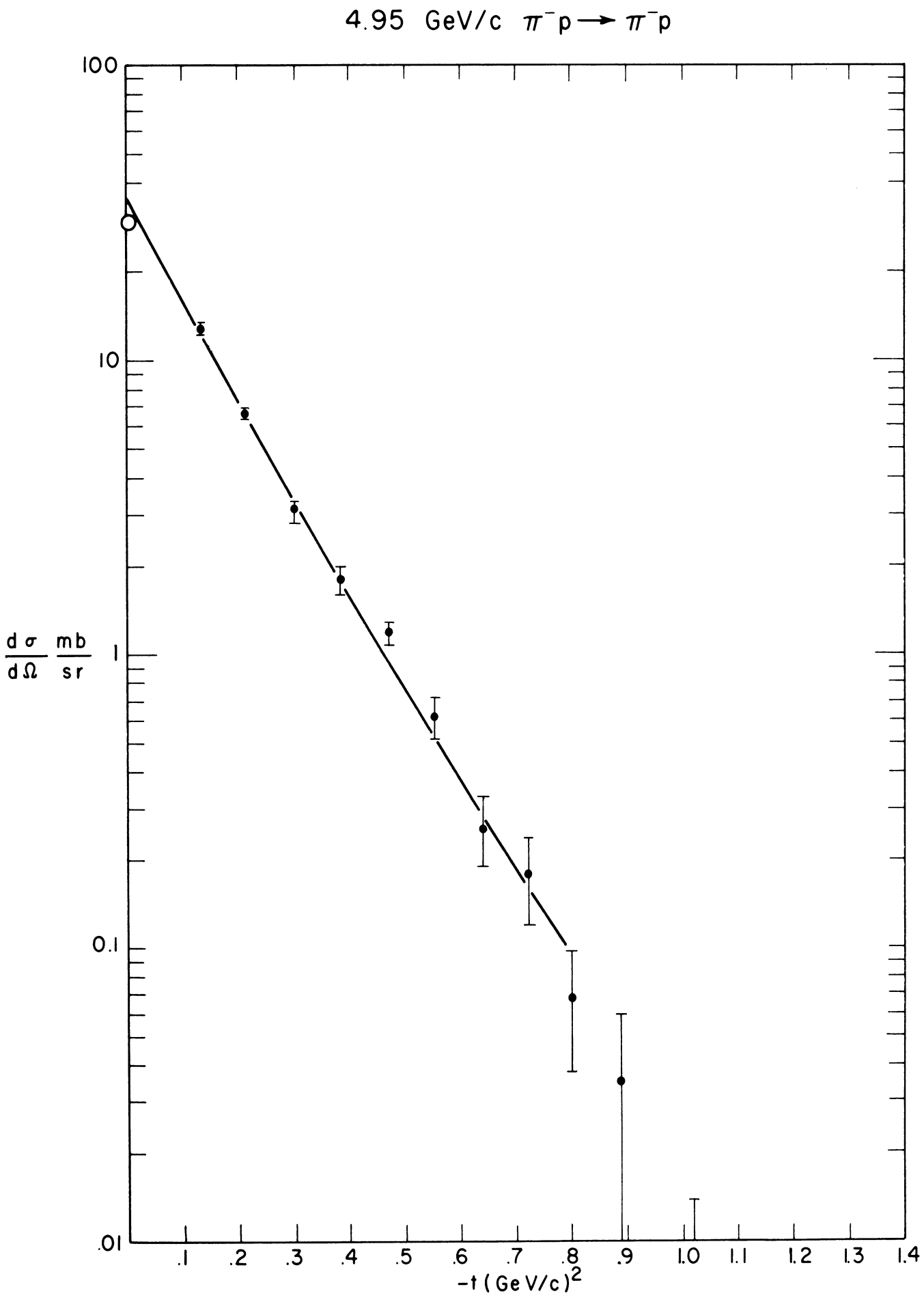
4.95 GeV/c $\pi^- p \rightarrow \pi^- p$
100
10
1
0.1
.01
$\frac{d\sigma}{d\Omega}\frac{mb}{sr}$
.1
.2
.3
.4
.5
.6
.7
.8
.9
1.0
1.1
1.2
1.3
1.4
$-t\,(GeV/c)^2$

Fig. 15

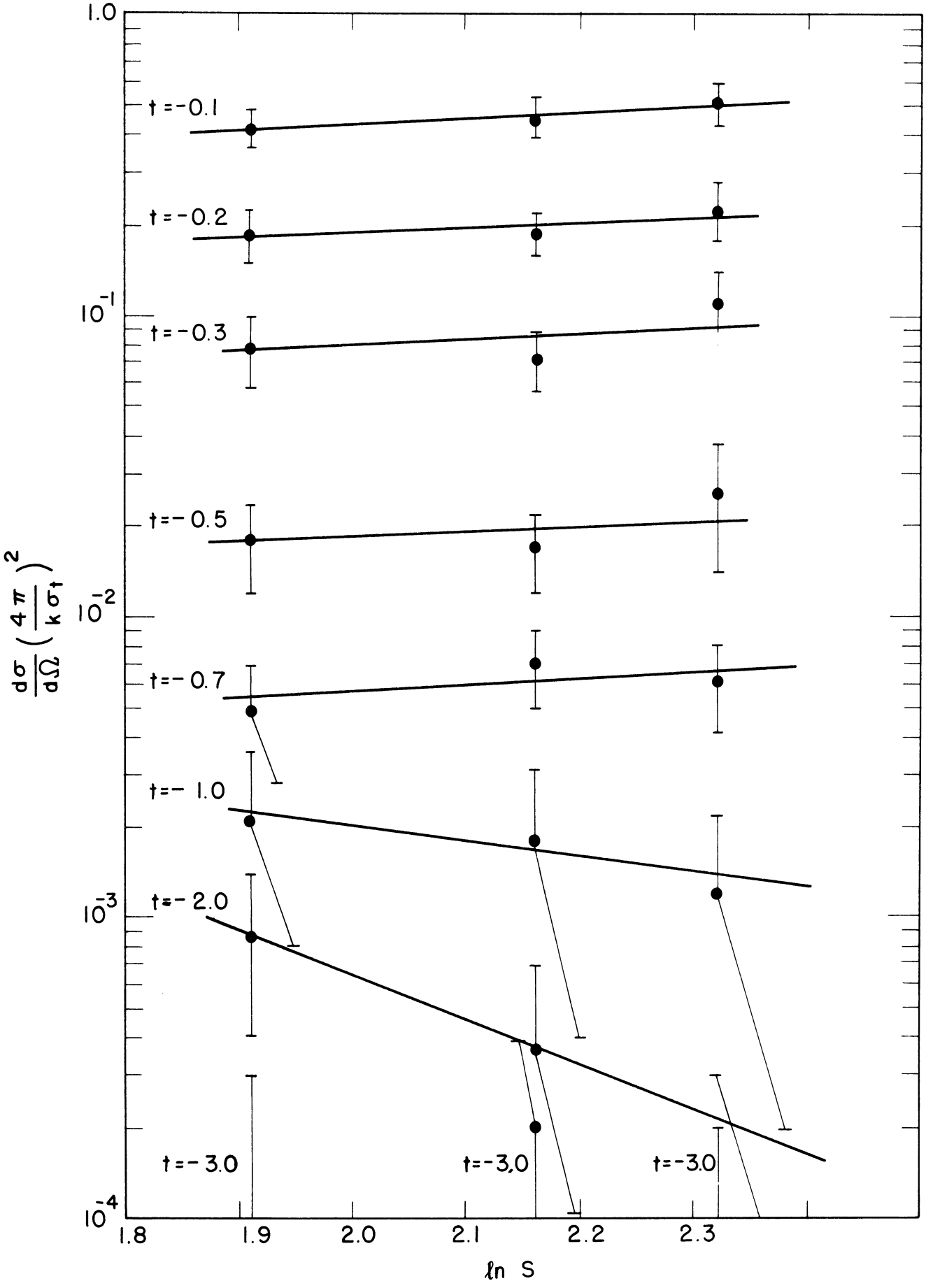
1.0
10^{-1}
10^{-2}
10^{-3}
10^{-4}
$\frac{d\sigma}{d\Omega}\left(\frac{4\pi}{k\sigma_t}\right)^2$
t=-0.1
t=-0.2
t=-0.3
t=-0.5
t=-0.7
t=-1.0
t=-2.0
t=-3.0
t=-3.0
t=-3.0
1.8
1.9
2.0
2.1
2.2
2.3
ln S

Fig. 16

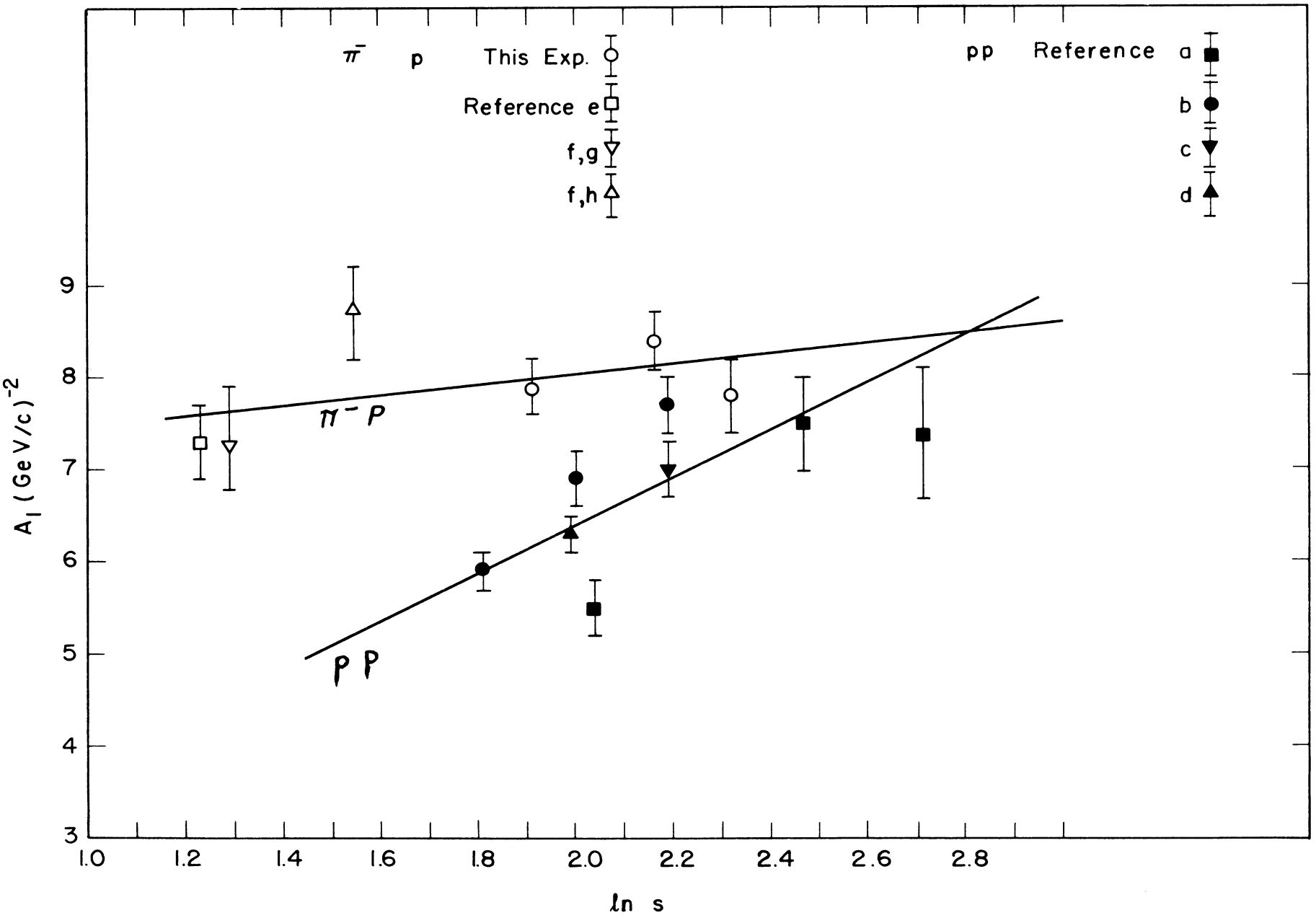
π⁻ p This Exp.
Reference e
f,g
f,h
pp Reference a
b
c
d
π⁻P
P P
A_1 (GeV/c)$^{-2}$
ln s
9
8
7
6
5
4
3
1.0
1.2
1.4
1.6
1.8
2.0
2.2
2.4
2.6
2.8

Fig. 17

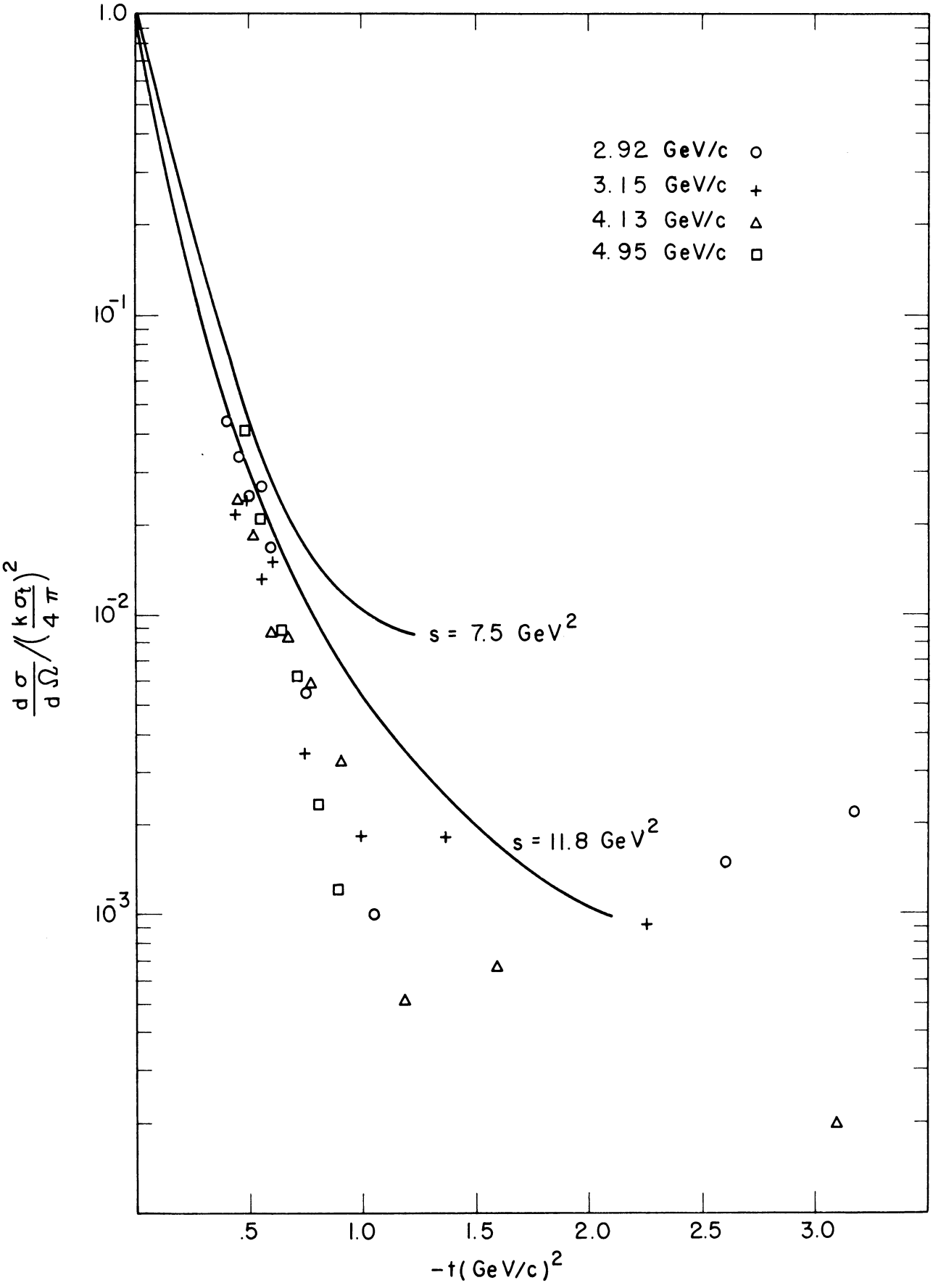
1.0
10^{-1}
10^{-2}
10^{-3}
$\frac{d\sigma}{d\Omega} / \left(\frac{k\sigma_t}{4\pi}\right)^2$
2.92 GeV/c o
3.15 GeV/c +
4.13 GeV/c △
4.95 GeV/c □
s = 7.5 GeV^2
s = 11.8 GeV^2
.5
1.0
1.5
2.0
2.5
3.0
$-t(\text{GeV/c})^2$

Fig. 18